J. Fluid Mech. (1977), *vol.* 81, *part* 1, *pp.* 155–185
Printed in Great Britain

Self-preserving turbulent wall jets over convex surfaces

By D. E. GUITTON AND B. G. NEWMAN
Department of Mechanical Engineering, McGill University, Montreal, Quebec

(Received 8 September 1975 and in revised form 22 December 1976)

The flow of an ostensibly two-dimensional wall jet over a logarithmic spiral has been studied both experimentally and theoretically. It is established that, if the skin friction is effectively constant, the flow may be self-preserving, and this is confirmed experimentally for the two spirals studied ($x/R = \frac{2}{3}$ and $x/R = 1$). The rate of growth has been predicted using the integral momentum equation and the integral equation for the combined mean and turbulent energy. Important assumptions in this theory are that the turbulence structure parameter $\overline{u'v'}/\overline{q'^2}$ and the normalized mean position of the superlayer are invariant with curvature, and the experiments show that this is nearly true. The growth is constant for each spiral and increases with curvature. Using the measured rate of growth, the integral energy equation gives a satisfactory prediction of the turbulent shear stress, but the two-dimensional integral momentum does not. The turbulence is very intense in these flows and the Reynolds stresses were corrected using correlations of up to fourth order. However, the corrections may still have been too small, which would account for some of the difference between the calculated and measured shear stress. The outer flow of a wall jet strongly influences the inner boundary layer and this effect is found to increase with curvature. The conventional logarithmic law of the wall ceases to apply for $x/R > \frac{2}{3}$.

1. Introduction

Self-preserving flows are of basic importance in the development of generalized calculation methods for turbulent shear flows, and those with curvature are of particular interest because even small curvature produces large changes in the flow structure and development (Bradshaw 1973). This paper is concerned with the flow of a two-dimensional incompressible jet in still surroundings over surfaces with a convex curvature which changes such that the outer part of the flow is self-preserving. Such surfaces are shown to be nearly logarithmic spirals. Turbulent mixing is increased by the convex curvature and the flow is therefore of interest as a means of increasing heat transfer, or increasing entrainment in an ejector. It is also of interest in the application of boundary-layer control by blowing as a means of energizing the boundary layer over aerofoils and flaps.

The jet emerges from a two-dimensional slot and flows over the convex surface. A boundary layer forms near the surface and the outer part of the flow resembles a half-jet (figure 1). The jet entrains the surrounding quiescent fluid and thus the maximum velocity decreases and the width of the flow increases downstream. The skin friction also has a minor effect. The pressure on the surface is lower than ambient and rises only slowly, so that the jet remains attached: this feature is usually called the Coanda effect (Newman 1961).

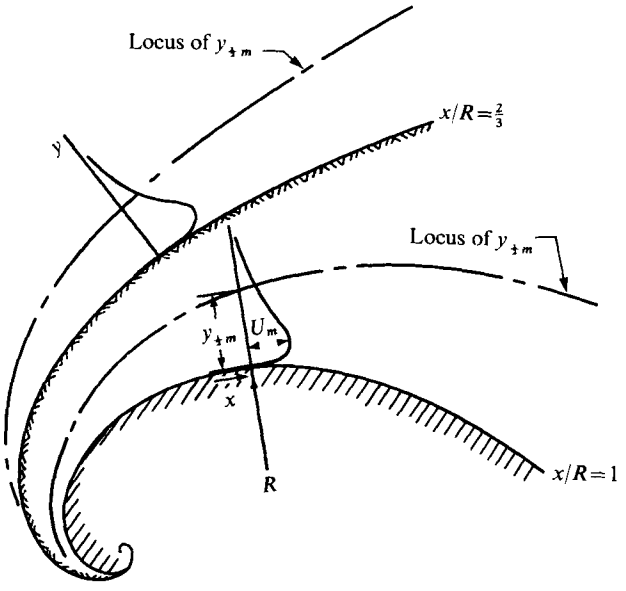

FIGURE 1. Schematic diagram of flow over logarithmic spirals. (Drawn to scale.)

Studies have been made on plane wall jets with still surroundings by Förthmann (1934), Sigalla (1958), Schwarz & Cosart (1961), Myers, Schauer & Eustis (1961), Gartshore & Hawaleshka (1964), Tailland & Mathieu (1967), Kohan (1968) and others. Much of the work followed Glauert's (1956) original analysis. Skin-friction measurements were specifically made by Parthasarathy (1964) and Alcaraz, Guillermet & Mathieu (1968). In all these measurements the length scale $y_{\frac{1}{2}m}$ varies linearly with downstream distance x and the maximum velocity U_m varies as x^a, where a is only slightly smaller than $-\frac{1}{2}$. Flows over curved surfaces of constant radius have been studied by Nakaguchi (1961), Newman (1961), Fekete (1963), Guitton (1964), Shridhar & Tu, (1969) and Spetel, Mathieu & Brison (1972). There exists only one detailed experimental study of self-preserving flow over logarithmic spirals (Giles, Hays & Sawyer 1966). An earlier investigation by Sawyer (1962) is included in that work. They measured the mean velocity and surface pressure on three convex logarithmic spirals ($x/R = \frac{1}{3}, \frac{2}{3}, 1$) and two concave ones ($x/R = -\frac{1}{3}, -\frac{2}{3}$), where R is the local radius of curvature. The Reynolds stresses and intermittency were measured on the most highly curved surface ($x/R = 1$).

A comparison of the maximum shear stress measured by Giles *et al.* on the $x/R = 1$ spiral with that calculated from the equations of motion reveals a discrepancy of over 45 %. There are three principal reasons for this.

(*a*) The two-dimensionality of their flows, as indicated by the shear stress distribution, is poor. It is shown in this paper (§ 3.2) that secondary flows and, in particular, slight irregularities in the slot lip can lead to large lateral variations of the jet thickness.

(*b*) The Reynolds stresses $\overline{v'^2}$ and $\overline{u'v'}$ were measured with a DISA X-wire (Type 55A38) probe and for this instrument Jerome, Guitton & Patel (1971) have shown that thermal-wake interference may cause significant errors.

(*c*) The anemometer signal was not linearized.

Thus the basic properties of self-preserving curved wall jets remain uncertain. The effects of curvature on the skin friction, the law of the wall, the turbulent shear stress at the maximum velocity and other turbulence properties need to be determined as a basis for predicting more complicated curved flows.

Integral theories have been developed to predict the effects of curvature on jets and wall jets. In such methods either the eddy viscosity or the mixing length is modified empirically to account for the curvature. The methods have been reviewed by Bradshaw (1973). Differential methods have only recently been applied to these flows. Morel (as reported by Bradshaw 1973) has modified the length scale in Bradshaw's modelling of the turbulent energy equation to account for curvature and has apparently predicted an increased growth for $x/R = \frac{1}{10}$, although the calculations have not been made for jets with still surroundings. Irwin & Smith (1975) have applied the Launder, Reece & Rodi (1973) model of the four equations for the individual components of the turbulence stress tensor in two-dimensional flow. They include the additional production terms due to curvature. They also make a correction to the pressure, velocity-gradient correlation in the equation for the shearing stress to account for the presence of a wall. The model equation for dissipation and the mean momentum equation are assumed to be unaffected by curvature. This theory therefore applies only for very small curvature (x/R less than about 0·08) but over this range predicts rates of growth in good agreement with the present measurements. The theory is particularly impressive in its ability to predict that the curvature effect on the rate of growth for a free jet is about one-tenth of that for a wall jet, which is in agreement with Smith's (1973) measurements.

In the present investigation two convex spirals have been used ($x/R = \frac{2}{3}, 1$). Particular care has been taken to establish flows that were two-dimensional in the mean. Skin friction has been measured with a heated element on the surface (Bellhouse & Schultz 1966; Brown 1967) and compared with Preston-tube readings to investigate the law of the wall. The mean velocity and the turbulence stress tensor were obtained from hot-wire readings corrected for the effects of high intensity turbulence, which is typically 50 % at $y_{\frac{1}{2}m}$. Intermittency in the outer part of the flow was also measured. A slot Reynolds number of about 3×10^4 was used in all experiments, including the comparative measurements on a plane, uncurved wall jet.

Integral theories for the mean velocity and surface pressure are presented. In addition, Townsend's (1970) theory, which is based on the flux of mean and turbulent energy integrated across the flow, is modified and applied to obtain a prediction for the rate of growth.

2. Theory

2.1. *Governing equations*

The time-mean momentum equations for two-dimensional turbulent flow over a curved wall of local radius R are (Goldstein 1938)

$$u\frac{\partial u}{\partial x}+\left(1+\frac{y}{R}\right)v\frac{\partial u}{\partial y}+\frac{uv}{R}=-\frac{1}{\rho}\frac{\partial}{\partial x}(p+\rho\overline{u'^2})-\left(1+\frac{y}{R}\right)\frac{\partial}{\partial y}\overline{(u'v')}-\frac{\overline{2u'v'}}{R} \qquad (1)$$

along the wall, in the direction x, and

$$u\frac{\partial v}{\partial x}+\left(1+\frac{y}{R}\right)v\frac{\partial v}{\partial y}-\frac{u^2}{R}=-\left(1+\frac{y}{R}\right)\frac{1}{\rho}\frac{\partial}{\partial y}(p+\overline{\rho v'^2})-\frac{\partial}{\partial x}\overline{(u'v')}+\frac{\overline{u'^2}-\overline{v'^2}}{R} \tag{2}$$

perpendicular to the wall, in the direction y.

In the above equations the mean velocity components are u and v in the x and y directions and dashes denote fluctuations about the mean. R is taken as positive for flow over a *convex* surface. The flow has been assumed to be incompressible. All viscous terms have been neglected, so that the equations apply everywhere except in the viscous sublayer.

The corresponding mean continuity equation is

$$\frac{\partial u}{\partial x}+\frac{\partial}{\partial y}\left[v\left(1+\frac{y}{R}\right)\right]=0. \tag{3}$$

If L_0 is a measure of the width of the wall jet, it is proposed to investigate flows which both conform to the boundary-layer approximation, so that $L_0/x \ll 1$, and are of small curvature, so that $L_0/R \ll 1$. R/x is of order 1. If the velocity component u is $O(1)$, v is $O(L_0/x)$ from (3). The dominant terms in (2), which are of order 1, are therefore

$$-\frac{u^2}{R}=-\frac{1}{\rho}\frac{\partial}{\partial y}(p+\overline{\rho v'^2}). \tag{4}$$

Since the pressure outside the wall jet is p_∞, $(p+\overline{\rho v'^2}-p_\infty)/\rho$ is $O(L_0/R)$. The pressure term in (1), $\rho^{-1}\partial(p+\overline{\rho u'^2})/\partial x$, is therefore $O(L_0/R)$ and is obtained with sufficient accuracy from the approximate equation (4).

2.2. *Self-preservation*

Consider the part of the wall jet outside the viscous sublayer as it proceeds over a convex surface (figure 1). It is self-similar for both the mean flow and the turbulent apparent stresses if

$$u=U_m f'(\eta), \quad -\overline{u'v'}=U_m^2 g_{12}(\eta), \quad \overline{u'^2}-\overline{v'^2}=U_m^2 g(\eta),$$

where

$$\eta=y/y_{\frac{1}{2}m}.$$

Since the region being investigated embraces part of the wall region it is implicitly assumed that $U_m \propto U_\tau$, where U_τ is the skin-friction velocity $(\tau_w/\rho)^{\frac{1}{2}}$. Thus the Reynolds number must be sufficiently large for the skin-friction coefficient $C_f=2(U_\tau/U_m)^2$ to be effectively independent of x.

The cross-flow velocity v is obtained by integrating the continuity equation (3) from $y=0$ ignoring the contribution of the viscous sublayer:

$$v\left(1+\frac{y}{R}\right)=-y_{\frac{1}{2}m}\left[\frac{dU_m}{dx}f-\frac{U_m}{y_{\frac{1}{2}m}}\frac{dy_{\frac{1}{2}m}}{dx}(\eta f'-f)\right], \tag{5}$$

where $f(0)=0$ by definition.

Integrating (4) from large y gives

$$\left[\frac{p}{\rho}+\overline{v'^2}\right]_\eta^\infty=\frac{y_{\frac{1}{2}m}}{R}U_m^2\int_\eta^\infty f'^2\,d\eta. \tag{6}$$

Substituting (5) and (6) into (1) and writing the resulting equation to order $y_{\frac{1}{2}m}/R$ yields

$$\frac{y_{\frac{1}{2}m}}{U_m}\frac{U_m}{dx}[f'^2-ff''+2g]-\frac{dy_{\frac{1}{2}m}}{dx}[ff''+\eta g']-g'_{12}$$
$$-\frac{y_{\frac{1}{2}m}}{R}\left\{\frac{y_{\frac{1}{2}m}}{U_m}\frac{dU_m}{dx}\left[ff'+1\int_\eta^\infty f'^2\,d\eta\right]+\frac{dy_{\frac{1}{2}m}}{dx}\left[ff'+\int_\eta^\infty f'^2\,d\eta\right]+[\eta g'_{12}+2g_{12}]\right\}=0. \quad (7)$$

This equation describes a self-preserving flow and thus all the terms outside the square brackets must be independent of x. It follows that

$$R\propto y_{\frac{1}{2}m}\propto x, \quad U_m\propto x^a,$$

where a is a constant. The surface defined by $R\propto x$ is a logarithmic spiral, which is given in polar co-ordinates by $r\propto e^{R\theta/x}$.

The exponent a may be found by integrating (1) across the flow. Multiplying (1) by $R+y$, using the continuity equation (3) and integrating from 0 to ∞ gives

$$\int_0^\infty (R+y)\frac{\partial}{\partial x}[u^2+p/\rho+\overline{u'^2}]\,dy=-R\frac{\tau_w}{\rho}.$$

Substituting for the pressure from (4) and ignoring the difference between $\overline{u'^2}$ and $\overline{v'^2}$ yields

$$\int_0^\infty\left(1+\frac{y}{R}\right)\frac{\partial}{\partial x}\left[u^2+\int_\infty^y\frac{u^2}{R}\,dy\right]dy=-\frac{\tau_w}{\rho},$$

which on rearranging and neglecting terms of order $(y_{\frac{1}{2}m}/R)^3$ becomes

$$\frac{d}{dx}\int_0^\infty u^2\,dy+\frac{1}{R^2}\frac{dR}{dx}\int_0^\infty yu^2\,dy=-\frac{\tau_w}{\rho}. \quad (8)$$

Substituting the self-preserving equations then gives

$$a=-\frac{1}{2}-\frac{C_f}{4\dfrac{dy_{\frac{1}{2}m}}{dx}\displaystyle\int_0^\infty f'^2\,d\eta}-\frac{\displaystyle\int_0^\infty \eta f'^2\,d\eta}{2\displaystyle\int_0^\infty f'^2\,d\eta}\frac{y_{\frac{1}{2}m}}{R}. \quad (9)$$

This differs from the value $a=-\frac{1}{2}$ given by Giles *et al.* for all values of $y_{\frac{1}{2}m}/R$ when $C_f=0$.

The surface pressure distribution on the logarithmic spiral is not obtained to sufficient accuracy by integrating (4). Integrating (2) across the flow gives

$$\frac{p_\infty-p_s}{\rho}=\int_0^\infty\frac{u^2}{R+y}\,dy-\int_0^\infty\frac{R}{R+y}u\frac{\partial v}{\partial x}\,dy-\int_0^\infty\frac{R}{R+y}\frac{\partial}{\partial x}\overline{(u'v')}\,dy$$
$$+\int_0^\infty\frac{R}{R+y}\overline{(u'^2-v'^2)}\,dy, \quad (10)$$

where p_s is the pressure on the surface. The last two terms are usually negligible for uncurved wall jets and will therefore be neglected. To order $(y_{\frac{1}{2}m}/R)^2$ the equation becomes

$$\frac{p_\infty-p_s}{\rho}=\int_0^\infty\frac{u^2}{R}\,dy-\int_0^\infty u^2\frac{y}{R^2}\,dy-\int_0^\infty u\frac{\partial v}{\partial x}\,dy.$$

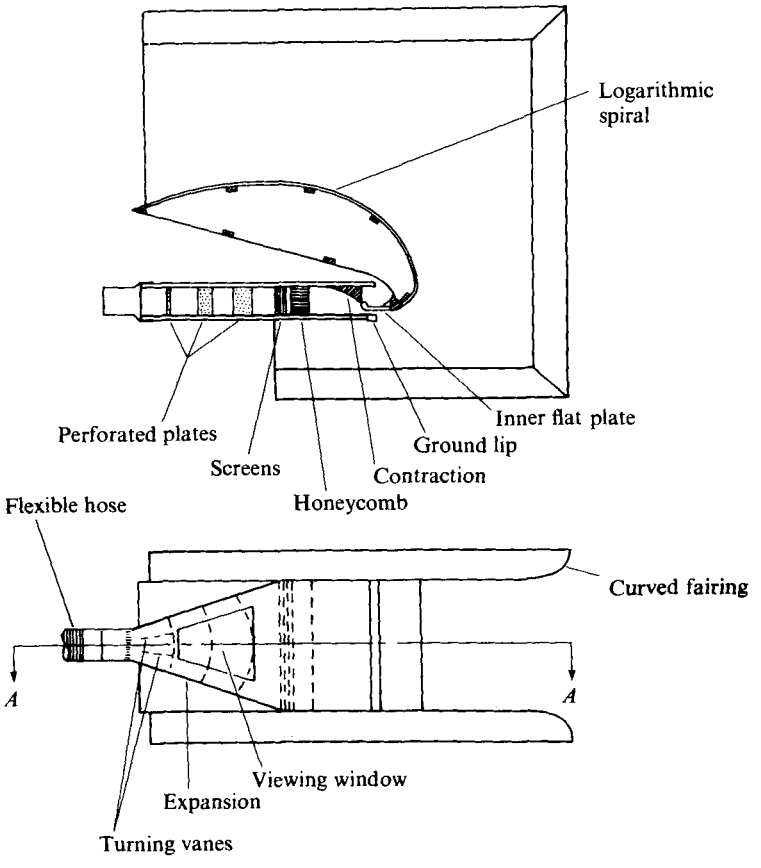

FIGURE 2. Experimental apparatus.

Substituting $u = U_m f'(\eta)$, using (5) and rearranging yields

$$\frac{p_\infty - p_s}{\rho U_m^2} = \frac{y_{\frac{1}{2}m}}{R}\left\{I_{02} - \frac{y_{\frac{1}{2}m}}{R}\left[I_{12} - \left(\frac{R}{x}\right)^2\left(\frac{a(a+1)}{2} I_{01} - (1+2a) I_{12}\right)\right]\right\}, \tag{11}$$

where $f(\infty) = I_{01}$. This and the other integrals

$$I_{02} = \int_0^\infty f'^2 d\eta, \quad I_{12} = \int_0^\infty \eta f'^2 d\eta$$

are computed from measured profiles and displayed in table 2. a is given by (9).

3. Experiment

3.1. *Experimental apparatus and procedure*

A detailed description of the experimental apparatus is given in Guitton (1970). It consisted of a 20 h.p. centrifugal blower supplying air through a flexible hose to an expansion chamber followed by a contraction leading to a high aspect ratio slot, $b = 0{\cdot}125$ in. wide and 24 in. long (see figure 2). The jet issuing from this slot flowed round a logarithmic spiral.

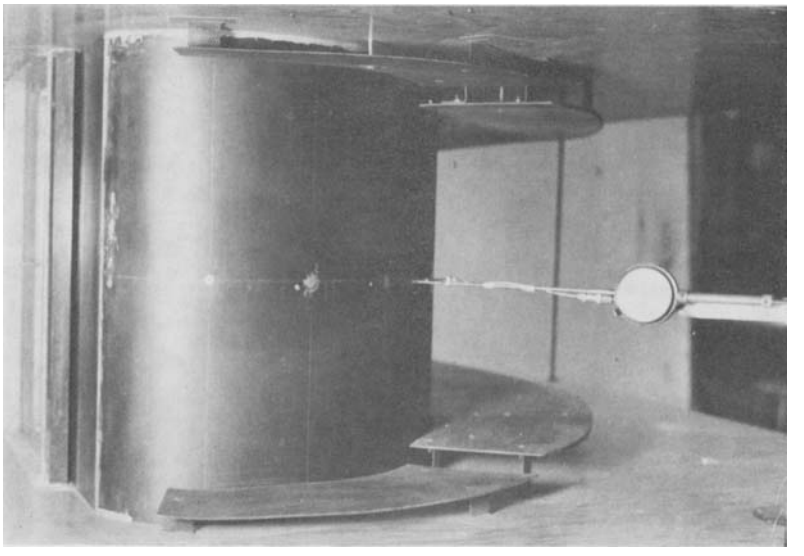

FIGURE 3. Experimental apparatus showing slot on left and traversing gear on right: $x/R = \frac{2}{3}$ spiral.

Two convex logarithmic spirals were constructed, $x/R = \frac{2}{3}$ and 1, and are similar to two of the spirals used by Giles *et al.* (1966). The surfaces were made of well-seasoned wood. The assembly of plenum chamber, slot and spiral was mounted between large end plates. A fairing was fitted around the edges of the end plates to prevent possible separation of the entrained air flow at the edges.

The flow from the slot was made uniform by fitting the upstream expansion chamber with vanes and perforated plates to eliminate separation, and gauze screens and honeycomb to further reduce spanwise irregularities. Experiments indicated that the uniformity of the jet was critically dependent on the condition of the edge of the slot lip (see § 3.2). It was therefore made from a specially annealed block of mild steel which was carefully ground and finally rubbed with blueing compound to prevent corrosion, especially of the sharp edge.

The inner wall of the slot was made from a $\frac{1}{2}$ in. thick, ground, mild-steel plate. The joint between the steel plate and the wooden surface of the spiral was carefully smoothed. It was impossible to place the jet too near the origin of a particular spiral for otherwise the downstream flow leaving the spiral would impinge on the hardware supplying the jet. The spirals were therefore joined to the steel plate at 0·85 and 2·26 in. from the spiral origin for $x/R = \frac{2}{3}$ and 1 respectively. In each case the length of the metal plate was determined experimentally to ensure that the virtual origin of the jet, found by extrapolating $y_{\frac{1}{2}m}$ to zero, coincided with the origin of the spiral. The required plates were 3 and 9 in. long for the cases $x/R = \frac{2}{3}$ and 1 respectively.

Air to the compressor was filtered to eliminate dust of size 1 μm or more: dust larger than about 1 μm settles on the wire and makes the hot-wire measurements inacccurate. The flow was controlled by a bleed valve which was followed downstream by a heat exchanger to control the jet air temperature, which was adjusted to equal that of the surroundings. The slot Reynolds number was set at $2{\cdot}8 \times 10^4$ for all tests.

The experimental apparatus for measuring the plane wall jet was that used by Gartshore & Hawaleshka (1964). The slot Reynolds number was set at $Re = 3 \times 10^4$ with a slot width of 0·300 in.

The mean velocity and Reynolds stresses were measured with either DISA type 55A25 normal or type 55A29 single-slanted wires (wire diameter 5μm, wire length about 1 mm) in conjunction with a type 55A01 anemometer. Normal wires were mounted parallel to the surface; slanted wires were mounted in a plane either normal or parallel to the surface depending on which Reynolds stresses were being measured. The traversing mechanism consisted of a long rod $\frac{3}{16}$ in. in diameter attached to a dial gauge at one end and passing through a bushing installed in the surface at the other end. The hot-wire probe was attached to the $\frac{3}{16}$ in. rod (see figure 3, plate 1) and the hot wire was set $2\frac{1}{2}$ in. upstream of the rod to minimize interference effects. Wires were calibrated before and after every traverse.

The signal from the anemometer was fed to a linearizer (Disa type 55D10). To measure mean velocity the linearizer output was connected to a voltage-to-frequency converter whose output was measured with a digital counter that integrated the signal over 1 min. To read the fluctuating signal the linearizer output was connected to a Hewlett Packard 3400 r.m.s. meter. Broadly speaking, r.m.s. values from the normal wire gave the longitudinal turbulence and the two readings from a slanted wire rotated through 180° about the mean velocity vector gave the Reynolds stresses in the plane of these measurements. However, corrections were applied to compensate for the usual

assumption that the turbulent fluctuations are linear perturbations from the mean condition. The intensity of the turbulence in convex curved jets is very high. (For example, at $y = y_{\frac{1}{2}m}$ on the $x/R = 1$ spiral the present measurements gave

$$(\overline{u'^2})^{\frac{1}{2}}/u = 0{\cdot}44.)$$

The correction terms were obtained by evaluating the wire response to fourth order in the velocity fluctuations (Guitton 1974). To evaluate these terms it was necessary to measure both third- and fourth-order turbulence correlations. This was done by using an X-wire (DISA, type 55A38) in conjunction with two DISA type 55A06 correlators.

The distance between the wire and the surface was accurately obtained by arranging that a cathode-ray oscilloscope be grounded when the probe touched a gauge block placed squarely on the surface. The dimensions of the wire probe were accurately obtained using an optical comparator.

The skin friction was measured with a hot-film probe (DISA type 55A92) calibrated in a pipe. The platinum film had an aspect ratio of 5 with the smaller length, 0·008 in., in the streamwise direction. In all tests the probe was held firmly in place, flush with the surface of interest, by means of a special mounting. Inaccuracies due to heat transfer to the surrounding surface were overcome using a novel transient technique (Guitton 1970). The hot-film probe was heated and maintained at constant temperature by the DISA 55A01 control unit. It was desired to compare the heated-element results with predictions obtained from Preston tubes and for this purpose six different tubes were made. All tubes were carefully ground and had a ratio of internal diameter to external diameter well over 0·2, the value above which, according to Head & Rechenberg (1962), the calibration becomes independent of the internal diameter. The skin friction was determined using the Patel (1965) calibration.

Intermittency was obtained by time differentiating the output of a normal hot wire and recording the resultant signal on light sensitive paper using a mirror galvanometer (frequency response $O(10^3\,\mathrm{Hz})$). A typical trace, say for $y = y_{\frac{1}{2}m}$, showed a relatively noiseless signal interrupted at random intervals by bursts of high frequency noise. The proportion of time that the trace was 'noisy' was taken to be a measure of the intermittency. Analysis of the same trace by independent observers indicated that the procedure gave values of mean and standard deviation repeatable to within roughly 5 %.

3.2. *The establishment of quasi-two-dimensional conditions*

A common method for verifying two-dimensionality is to compare velocity profiles measured at various stations off the centre-line. A less qualitative approach is to verify that the velocity and length scales that describe the flow vary downstream in a manner consistent with the two-dimensional integral momentum equation for the complete flow. The most sensitive technique, however, is to compare the distribution of measured shear stress with that calculated from the momentum equation using the mean velocity measurements, a procedure which becomes easily manageable for self-preserving flows.

The inadequacy of the first, qualitative procedure can be demonstrated by examining a plane wall jet in still air which has a small flow divergence with collateral streamlines associated with a source. For convenience the source is assumed to be about 10^4 slot widths upstream of the slot. Using the x-momentum integral equation

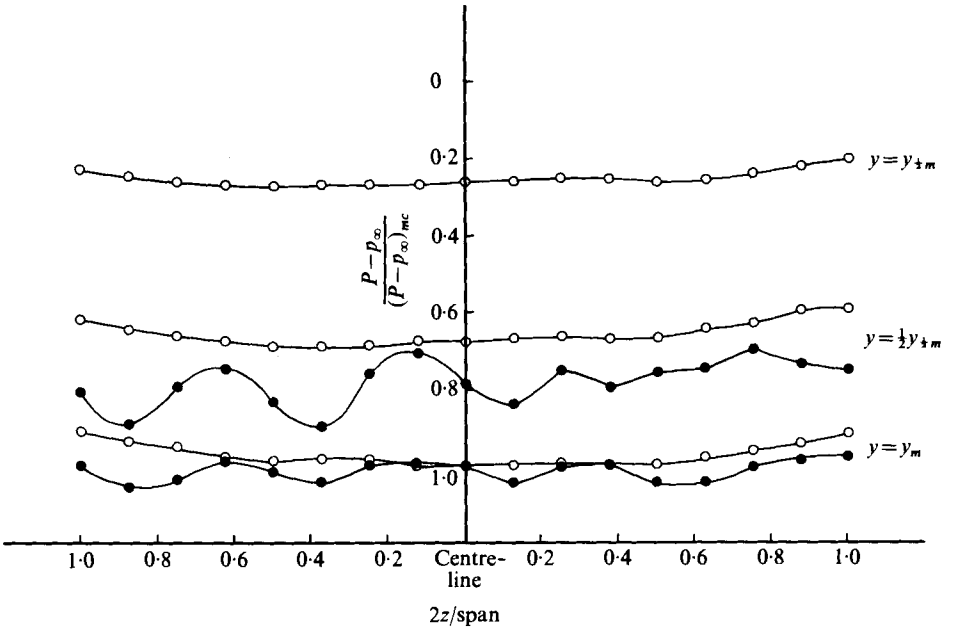

FIGURE 4. Lateral variation of total head measured at $x = 6{\cdot}4$ in. at three different distances away from the $x/R = \frac{2}{3}$ spiral surface. ●, with sharp knife edge slot lip; ○, after honing lip to form a sharp 90° corner.

on the centre-line, the additional term due to cross-flow is then equal to about half the skin-friction term. Thus calculating skin friction, and with it the shear-stress distribution, from only the two-dimensional integral momentum equation yields values which are about 50 % in error. It is worth noting however that such an error in skin friction leads to about a 3 % error in the exponent a, so that the maximum velocity decay is not much affected by such small three-dimensional effects.

It is extremely difficult to obtain satisfactory two-dimensional curved flow and it is therefore worth recording our efforts to do this in some detail. First, it should be noted that we were only partially successful. Even in the final configurations, U_m calculated via the two-dimensional momentum equation was only within 2 % of the experimental value and the maximum measured shear stress was still 25 % lower than the calculated value.

The tendency for the flows to depart from two-dimensionality can be traced to two sources: one is related to conditions at the slot lip or within the plenum chamber leading to the slot and the other is due to secondary flows originating in the boundary layers on the end plates.

It has been known for some time that small imperfections of the slot lip can have a detrimental effect on two-dimensionality (Fekete 1963). The prototype of the present apparatus was designed with this difficulty in mind. The slot lip was shaped like a knife edge, carefully ground, and the wall leading to it was straight and free of obstructions. Nevertheless the initial measurements revealed a flow of poor quality (figure 4). In these measurements a Pitot tube was moved parallel to, and at various distances from, the surface.

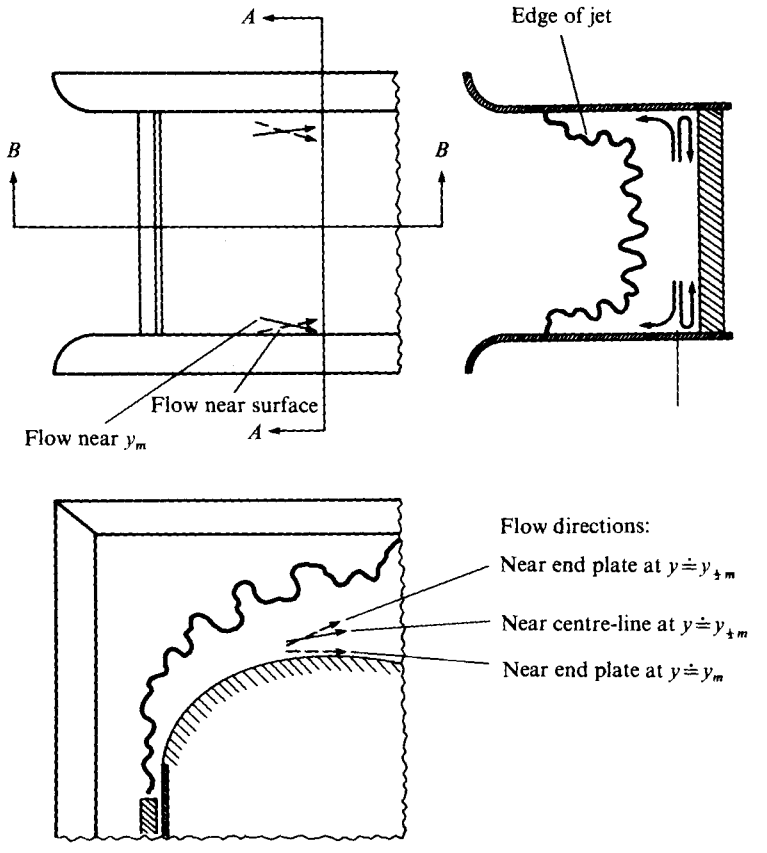

FIGURE 5. Schematic diagram of observed flow directions.

A number of tests were conducted in an attempt to trace the source of these flow imperfections. The flow in the expansion was not separated. Placing pieces of masking tape across the honeycomb so as to crudely alter the flow distribution had no effect. Similarly, placing obstructions on both sides of the plenum chamber just upstream of the slot had a negligible effect on the transverse flow distribution. Surprisingly a remarkable improvement in the flow (figure 4) was obtained after the knife edge had been honed flat so as to form a sharp 90° corner. On a convex surface a thick region of flow at a certain spanwise position tends to grow relative to an adjacent thin region because the surface pressure under the former is lower and there is thus lateral flow from the thin region to the thick region. Small initial irregularities may therefore be amplified. A source of such irregularities is variation of the position of separation from the slot *lip* due to minute variations of lip geometry. Such variations are more easily controlled when manufacturing a 90° corner.

The second source of difficulty relates to secondary flows near the end plates. Figure 5 shows schematically some flow directions detected with smoke and tufts. Near the end plates the surface flow on the spiral is directed towards the centre-line, indicating that the static pressure is higher near the corners. Not far above the curved surface (near y_m) the secondary flow is directed away from the centre-line, and at the end plate it appears to split into two parts: one forming a flat vortex in the inner

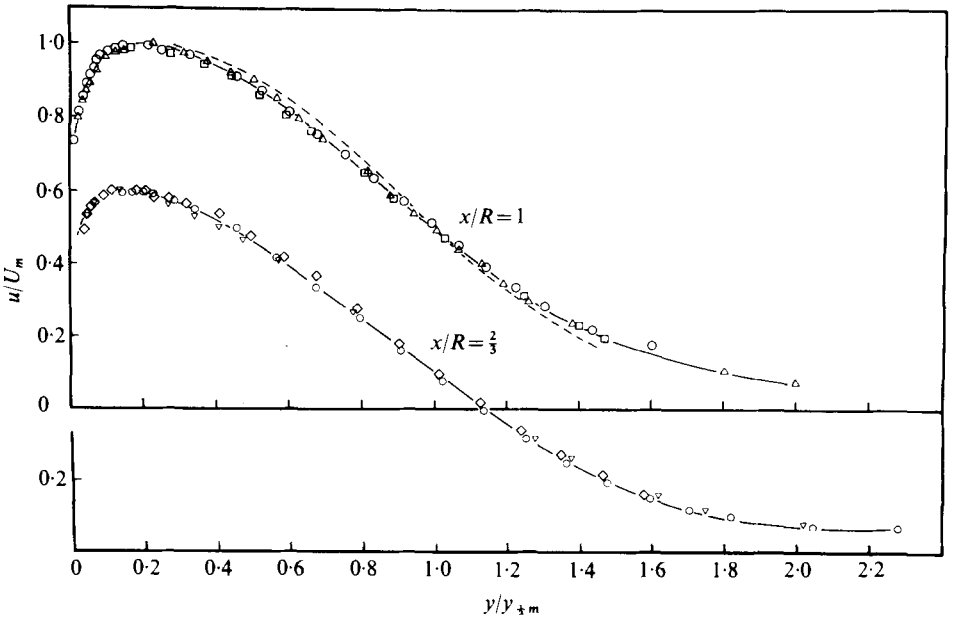

FIGURE 6. Mean velocity profiles. For $x/R = \frac{2}{3}$: ○, $x = 5{\cdot}4$ in.; ▽, $x = 19{\cdot}6$ in.; ◇, $x = 28{\cdot}7$ in.; ——, mean line through data. For $x/R = 1$: ○, $x = 16{\cdot}0$ in.; □, $x = 19{\cdot}9$ in.; △, $x = 29{\cdot}8$ in.; ——, mean line through data; – – –, measurements of Giles *et al.* (1966).

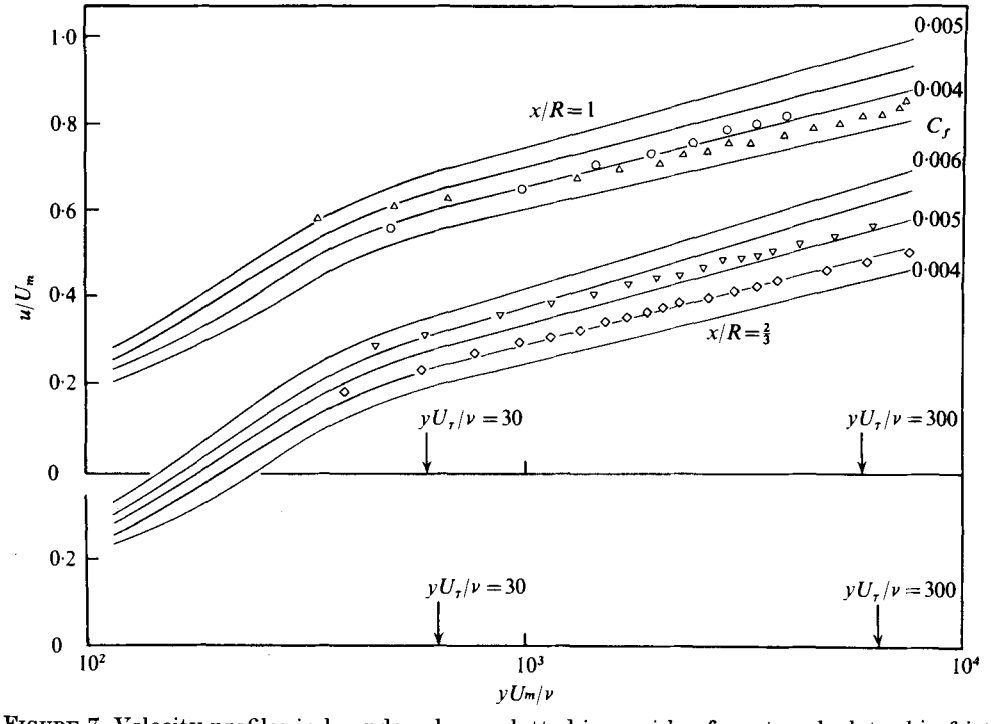

FIGURE 7. Velocity profiles in boundary layer plotted in semi-log form to calculate skin friction assuming existence of a law of the wall with constants $A = 5{\cdot}5$ and $B = 5{\cdot}45$ (method of Clauser). For $x/R = \frac{2}{3}$: ▽, $x = 13{\cdot}3$ in; ◇, $x = 28{\cdot}7$ in. For $x/R = 1$: ○, $x = 14{\cdot}3$ in; △, $x = 29{\cdot}8$ in.

	C_f	Position
	Plane wall jet	
Hot film	0·00600	x = 27 in.
Preston tube†	0·00555	$\frac{y_m U_m}{\nu} = 0{\cdot}99 \times 10^4$
Clauser plot‡	0·00570	
Hot film	0·00524	x = 42 in.
Preston tube†	0·00514	$\frac{y_m U_m}{\nu} = 1{\cdot}57 \times 10^4$
Clauser plot‡	0·00530	
Hot film	0·00473	x = 62 in.
Preston tube†	0·00486	$\frac{y_m U_m}{\nu} = 1{\cdot}87 \times 10^4$
Clauser plot‡	0·00500	
	$x/R = \frac{2}{3}$	
Hot film	0·00515	x = 13·3 in.
Preston tube†	0·00515	$\frac{y_m U_m}{\nu} = 2{\cdot}1 \times 10^4$
Clauser plot‡	0·00530	
Hot film	0·00526	x = 19·6 in.
Preston tube†	0·00488	$\frac{y_m U_m}{\nu} = 2{\cdot}54 \times 10^4$
Clauser plot‡	—	
Hot film	0·00444	x = 28·7 in.
Preston tube†	0·00510	$\frac{y_m U_m}{\nu} = 2{\cdot}73 \times 10^4$
Clauser plot‡	0·00450	
	$x/R = 1$	
Hot film	0·00540	x = 14·3 in.
Preston tube†	0·00448	$\frac{y_m U_m}{\nu} = 4{\cdot}04 \times 10^4$
Clauser plot‡	0·00407	
Hot film	0·00513	x = 29·8 in.
Preston tube†	0·00417	$\frac{y_m U_m}{\nu} = 6{\cdot}06 \times 10^4$
Clauser plot‡	0·00380	

† Average of five tubes.
‡ For log-law constants $A = 5{\cdot}5$, $B = 5{\cdot}45$.

TABLE 1. Comparison of skin friction measured with hot film, Preston tube and Clauser plot.

layer and the other contributing to the rapid expansion of the boundary-layer flow. The rapid expansion of the side flow creates a U-shaped wall jet in which the side flow becomes so large that it may encroach upon the central flow. This type of secondary flow differs from that which occurs in a curved rectangular channel. In a channel the pressure gradient imposed on the boundary layers which form on the two plane side walls is balanced by an increased curvature of the slower-moving fluid there, and consequently the flow along these walls has an additional component of velocity directed *towards* the centre of curvature of the channel.

The principal objective was to minimize this problem, and consequently no detailed experiments were made to determine its precise nature. The technique finally adopted was to add a number of small end plates arranged in a ladder formation so that each succeeding end plate cut off the boundary layer formed immediately upstream of it (see figure 3). An attempt was made to limit the number of end plates in order to minimize blockage and brief trials indicated that a 'ladder' consisting of three end

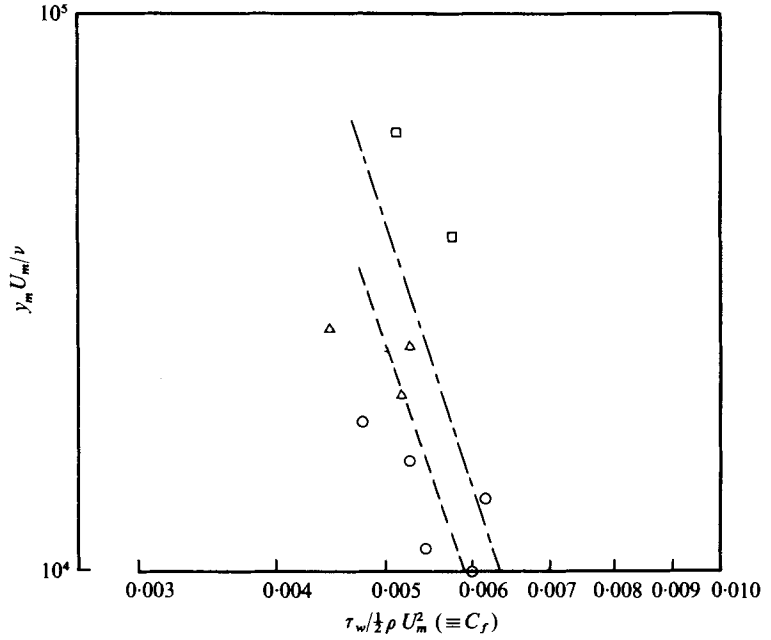

FIGURE 8. Effect of curvature on the relation between C_f and the Reynolds number $y_m U_m/\nu$. ○, plane wall jet; △, $x/R = \frac{2}{3}$; □, $x/R = 1$. Other data for plane wall jet: – – –, Alcaraz *et al.* (1968); — – —, Escudier *et al.* (1966).

plates would be satisfactory for the downstream extent of the present measurements. The position of each end plate was determined by trial and error.

4. Discussion of results and comparison with theory

The mean velocity profiles, as measured with hot wires and corrected for high intensity turbulence, are shown for the two spirals $x/R = \frac{2}{3}$ and 1 in figure 6. The results are seen to collapse onto a single curve when non-dimensionalized using $y_{\frac{1}{2}m}$ and U_m. The similarity extends well into the boundary-layer region and the value of $y_m/y_{\frac{1}{2}m}$ is constant in each case, becoming larger as the surface curvature is increased. The results of Giles *et al.* for $x/R = 1$ are also shown and the disagreement with the present measurements is noteworthy.

In figure 7 the results for the inner boundary-layer region are plotted in logarithmic form in the manner proposed by Clauser (1954). In these figures the universal log law proposed by Patel (1965) has been assumed:

$$u/U_\tau = 5{\cdot}5 \log (yU_\tau/\nu) + 5{\cdot}45.$$

The results for two stations are shown in each case. Such a presentation is extremely sensitive to errors in y, and errors of $\pm 0{\cdot}001$ in. were certainly possible. For all the points of interest the distance from the wall exceeded 100 wire diameters, so that there was no significant additional heat loss due to the presence of the wall. From these curves a logarithmic region can be discerned for $30 < yU_\tau/\nu < 300$ and the value of the skin friction may be estimated. The values may be compared with those obtained using

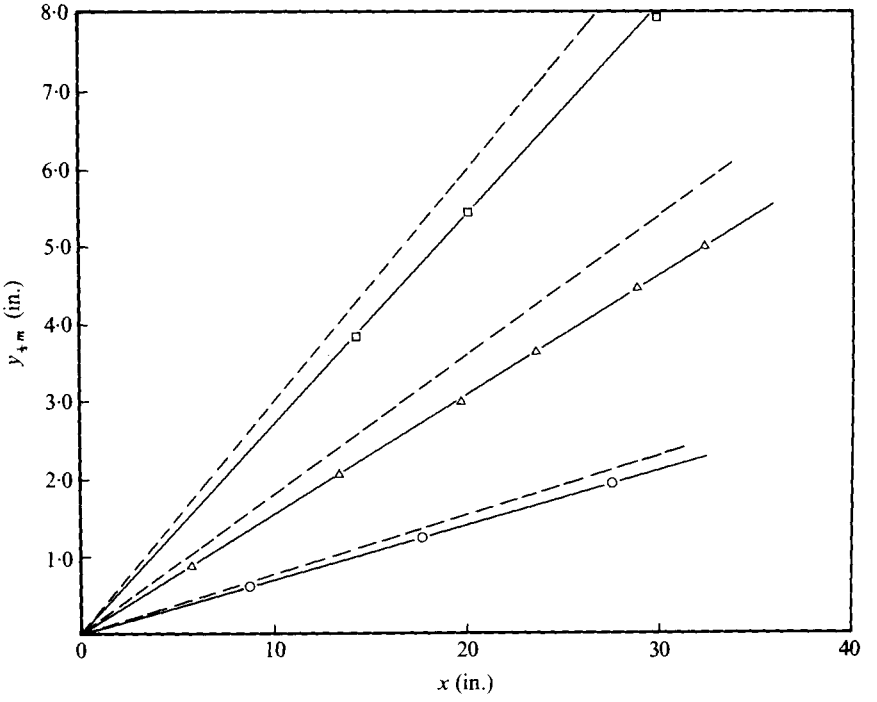

FIGURE 9. Effect of curvature on the linear growth rate. ○, plane wall jet; △, $x/R = \frac{2}{3}$; □, $x/R = 1$; – – –, measurements of Giles *et al.* (1966).

Preston tubes and with values obtained from the heated elements: they are given in table 1. For the $x/R = \frac{2}{3}$ spiral the agreement is satisfactory although a fixed error in y is apparent for the mean velocity measurements at $x/b = 106$. The log law appears to be valid for the boundary layer on this surface. For the $x/R = 1$ spiral the agreement is less satisfactory, the heated-element results being significantly larger than the others. It is possible that the conventional logarithmic law of the wall no longer applies owing to the curvature of the flow. This disagreement *cannot* be convincingly attributed to the adverse pressure gradient because $(\nu/\rho U_\tau^3)\,dp/dx = 0{\cdot}0015$, which is significantly less than the value 0·01 quoted by Patel (1965) for an adverse pressure gradient.

The heated-element measurements of skin friction are plotted logarithmically against $y_m U_m/\nu$ in figure 8. The present results for a plane wall and the two logarithmic spirals are shown. The dashed line is the best fit to the balance measurements of Alcaraz *et al.* (1968) for a plane wall jet, and the chain-dotted line is that given by Escudier, Nicoll & Spalding (1966) for the same case. The agreement with Alcaraz *et al.* is well within the scatter of their data. It is noted that the skin-friction coefficient for a given $y_m U_m/\nu$ is significantly increased by the curvature as might be expected.

Evidence that each flow was self-preserving is now presented. The half-width $y_{\frac{1}{2}m}$ is plotted against x in figure 9. The results lie convincingly on straight lines with the origin of the jet growth coinciding with the origin of the spiral in those two cases. The rates of growth are significantly less than those measured by Giles *et al.*, who used apparatus of lower aspect ratio. Their measurements are considered to be less accurately two-dimensional than ours because the agreement between measured shear and that

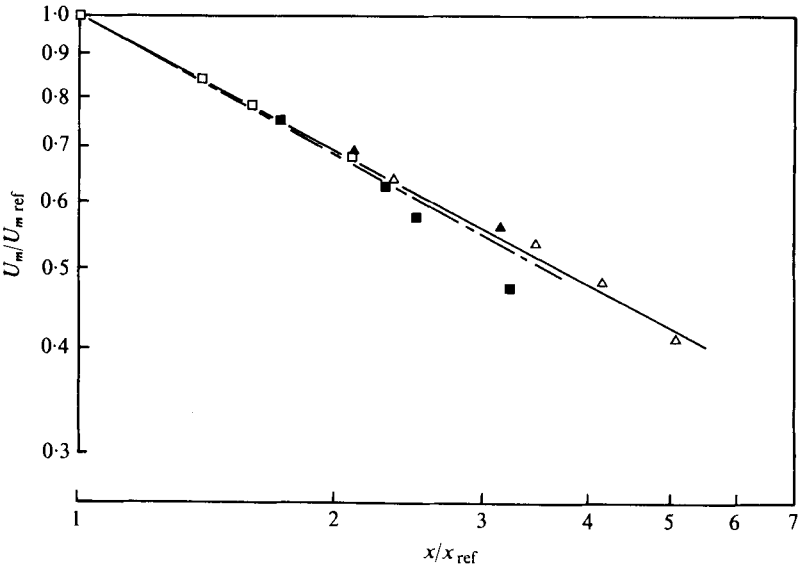

FIGURE 10. Streamwise variation of maximum velocity. △, $x/R = \frac{2}{3}$; □, $x/R = 1$; ——, $U_m/U_{m\mathrm{ref}} = (x/x_{\mathrm{ref}})^{-0\cdot535}$; — — —, $U_m/U_{m\mathrm{ref}} = (x/x_{\mathrm{ref}})^{-0\cdot571}$. Data of Giles *et al.* (1966) for same spirals are represented by filled symbols.

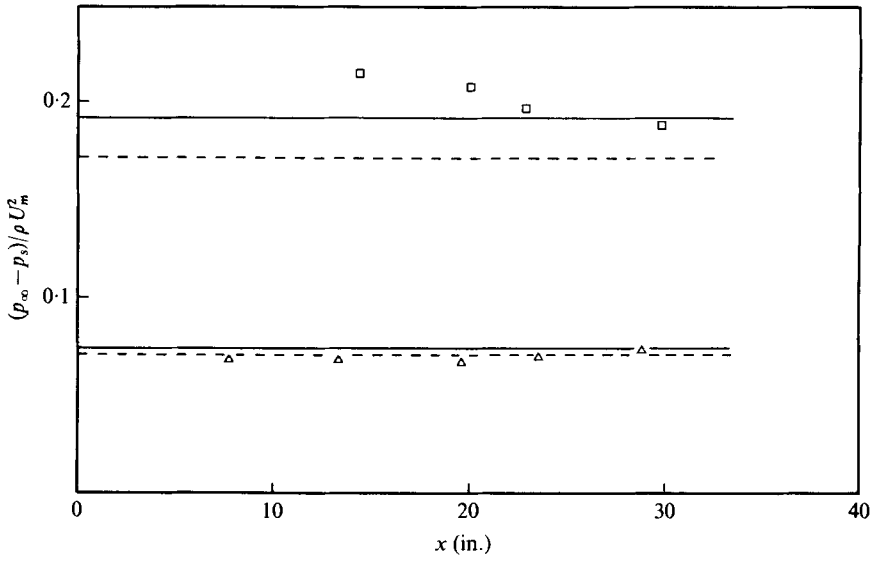

FIGURE 11. Streamwise variation of the surface pressure. △, $x/R = \frac{2}{3}$; □, $x/R = 1$; ——, calculated from full y-momentum equation (11); – – –, calculated from (11). Logarithmic scales.

calculated from the rate of growth is significantly worse (see § 3.2). However, the discrepancies are less than those of previously published data for the plane wall jet in still surroundings. Kohan (1968) has reviewed these data and quotes values of $dy_{\frac{1}{2}m}/dx$ ranging from 0·06 to 0·08 for slot Reynolds numbers greater than $1{\cdot}2 \times 10^4$.

Values of $U_m/U_{m\mathrm{ref}}$ are plotted logarithmically against x/x_{ref} in figure 10 and lie convincingly on a straight line in each case. It was necessary to use a reference station

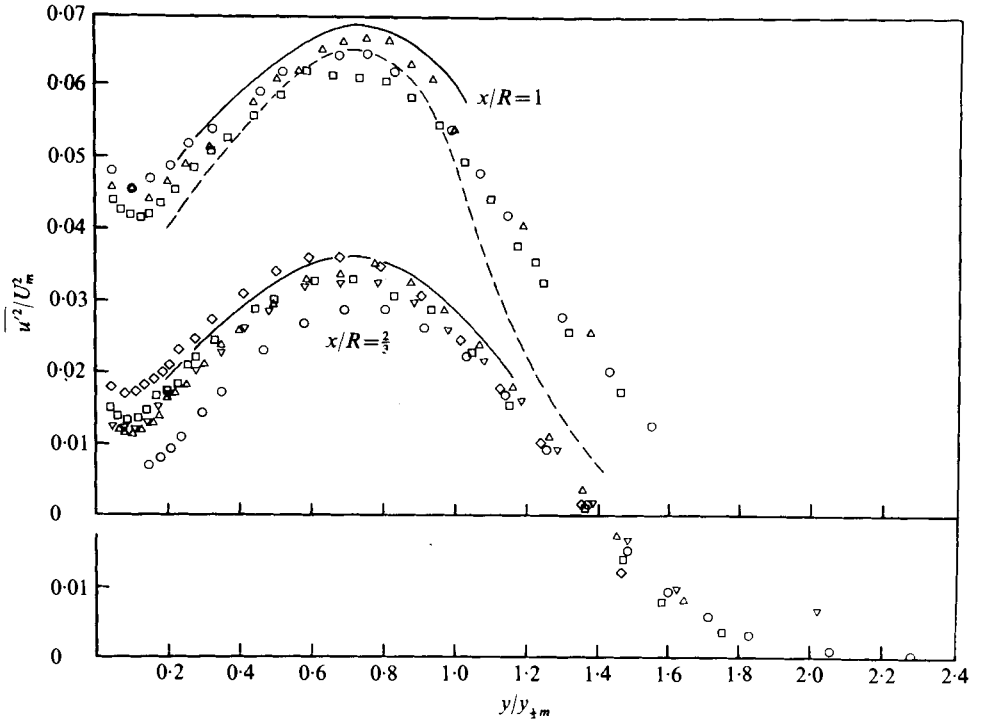

FIGURE 12. Intensity of u' fluctuation across the jets. For $x/R = \frac{2}{3}$: ○, $x = 5{\cdot}7$ in.; △, $x = 13{\cdot}3$ in.; ▽, $x = 19{\cdot}6$ in.; □, $x = 23{\cdot}5$ in.; ◇, $x = 28{\cdot}7$ in.; ——, mean curve through the experimental points corrected for high intensity. For $x/R = 1$: ○, $x = 14{\cdot}3$ in.; □, $x = 19.9$ in.; △, $x = 29{\cdot}8$ in.; ——, mean curve through the experimental points corrected for high intensity; – – –, measurements of Giles *et al.* (1966).

in presenting these results because of the somewhat arbitrary position of the slot in relation to the origin of the spiral. The predicted slopes calculated from (9), using the heated-element values of C_f, are shown and have been tied to the first experimental point in each case. Agreement is good for $x/R = \frac{2}{3}$, but the predicted slope is somewhat larger than the measured value for $x/R = 1$.

The measured surface pressure p_s is plotted as $(p_\infty - p_s)/\rho U_m^2$ against x in figure 11. For a self-preserving flow it should be constant in each case. The value predicted to order $(y_{\frac{1}{2}m}/R)^2$ by (11) (using (9) for a) is also shown. Agreement is very good for $x/R = \frac{2}{3}$. For $x/R = 1$ it is less satisfactory and this can be attributed partly to the higher curvature, since a better prediction is obtained when the pressure is calculated from the full momentum equation (solid lines in figure 11).

$\overline{u'^2}/U_m^2$ is shown in figure 12 for the two cases. For $x/R = \frac{2}{3}$ it is interesting to note that the flow at the upstream station is not self-preserving for $\overline{u'^2}$ over the inner half of the flow, even though it is self-preserving for the mean velocity there. The solid lines on the figure represent the mean curve through the experimental points corrected for high intensity turbulence. The dashed curve represents the measurements of Giles *et al.* for $x/R = 1$; the discrepancy for large $y/y_{\frac{1}{2}m}$ may be partly attributed to their use of a non-linearized hot-wire anemometer. It is noted that the longitudinal turbulence is generally higher for the larger curvature. The corresponding curves for $\overline{v'^2}/U_m^2$ and

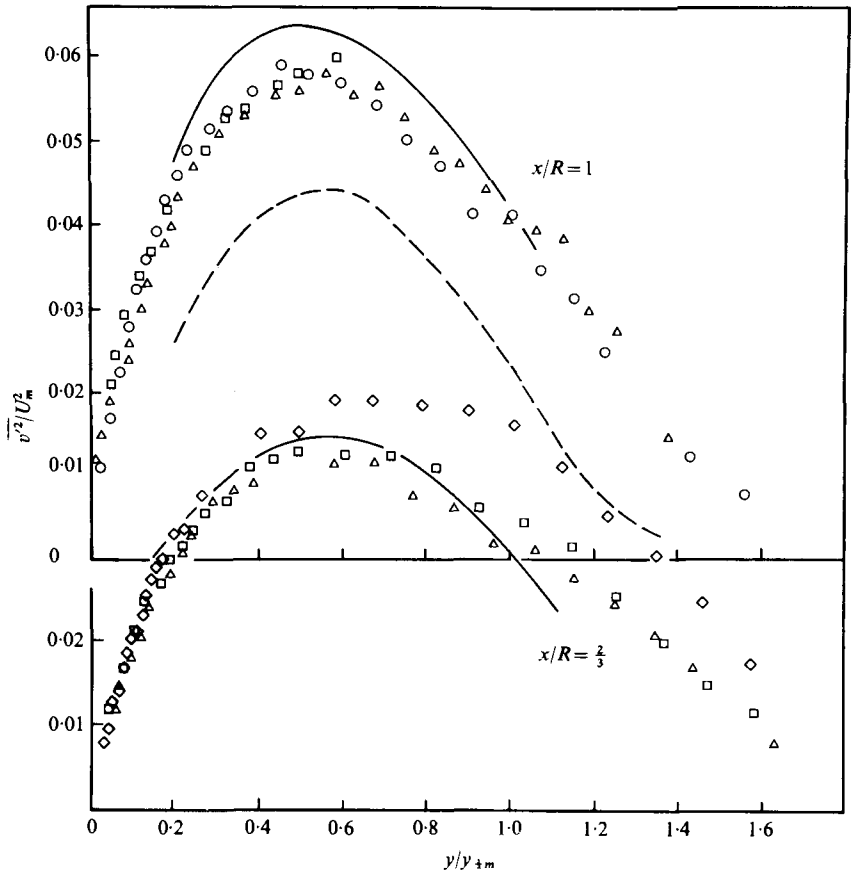

FIGURE 13. Intensity of v' fluctuation across the jets. Symbols as in figure 12.

$\overline{w'^2}/U_m^2$ are shown in figures 13 and 14 with the solid curves again representing the mean curve corrected for high intensity effects. The increased turbulence level for $x/R = 1$ is again noted. It is particularly noticeable in the mean curves for twice the turbulence energy $\overline{q'^2}/U_m^2 = (\overline{u'^2}+\overline{v'^2}+\overline{w'^2})/U_m^2$ shown in figure 15, where measurements in a plane wall jet are also presented. The deviation of results for $\overline{v'^2}/U_m^2$ and $\overline{w'^2}/U_m^2$ for $x/R = \frac{2}{3}$ at the far-downstream station in figures 13 and 14 is attributed partly to three-dimensional effects and partly to inaccuracies in the measurement of intense turbulence. Surprisingly, such a discrepancy is not noticeable for $\overline{v'^2}/U_m^2$ on the $x/R = 1$ spiral and there may have been a cancellation of errors in this case. The measurements by Giles *et al.* are also shown and are much lower. The disagreement is attributed partly to their use of cross-wires with thermal-wake interference (Jerome *et al.* 1971). They did not measure $\overline{w'^2}/U_m^2$.

The turbulent shear stresses $\overline{u'v'}/U_m^2$ are shown in figures 16 and 17. The results again collapse quite well onto single curves for each case, and the solid lines show the mean values corrected for high intensity turbulence. The starred points are values calculated from the x-momentum equation (1) using the static pressure from (4). They are seen to be significantly higher. This discrepancy is attributed to a slight divergence

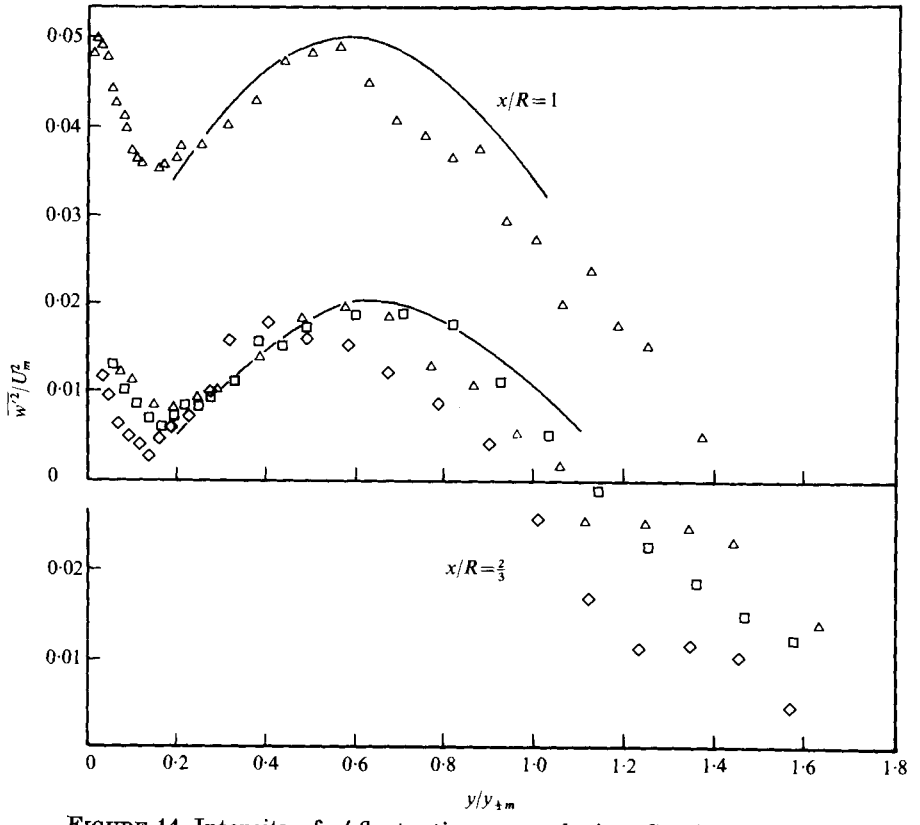

FIGURE 14. Intensity of w' fluctuation across the jets. Symbols as in figure 12.

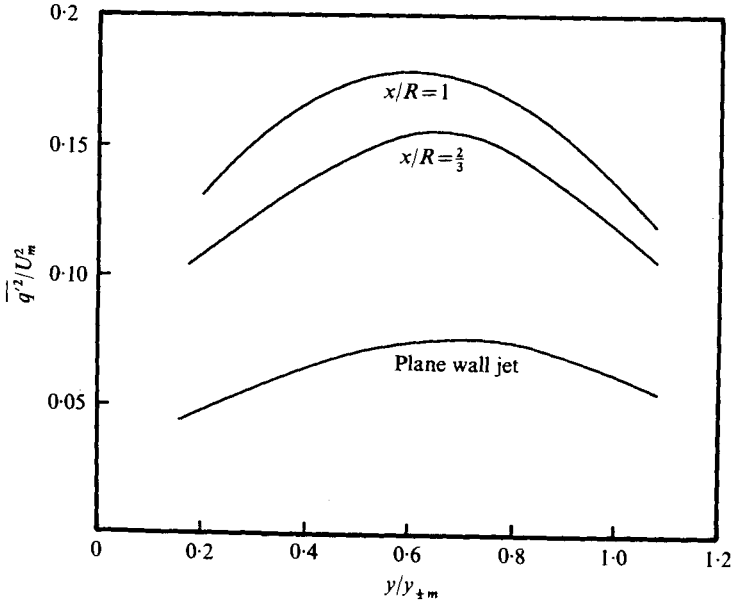

FIGURE 15. Effect of curvature on the distribution of $\overline{q'^2}/U_m^2$ across the jets.

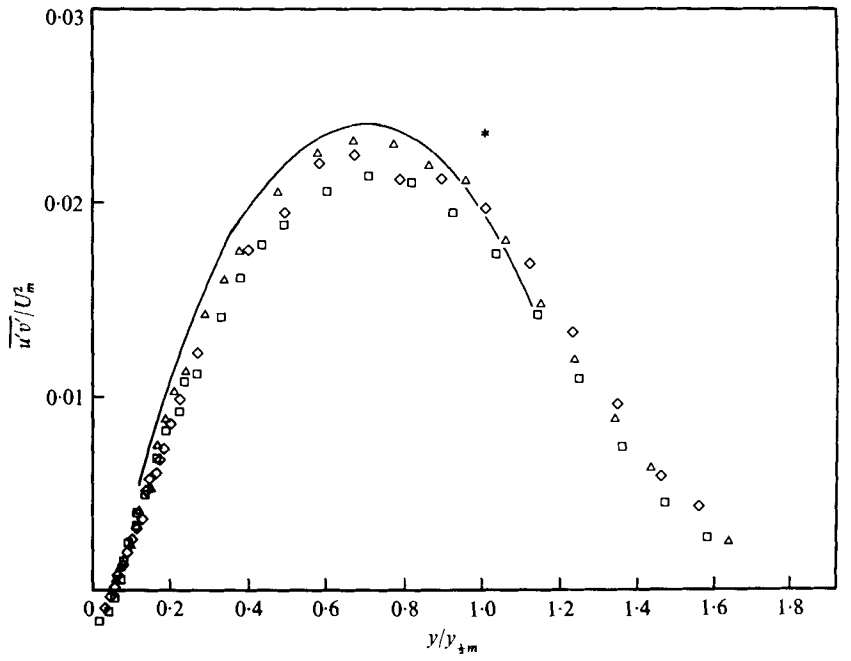

FIGURE 16. Shear-stress distribution across the jet, $x/R = \frac{2}{3}$. *, calculated from momentum equation; △, $x = 13{\cdot}3$ in.; □, $x = 23{\cdot}5$ in.; ◇, $x = 28{\cdot}7$ in.; ——, mean curve through experimental points corrected for high intensity.

of the flow from truly two-dimensional conditions, a divergence which does not significantly affect the turbulence but gives errors in the calculated shearing stress (see § 3.2 for further details). In figure 17 the measurements of Giles *et al.* are shown to be in good agreement with the present measurements for the inner part of the flow, but to deviate significantly in the outer part, where the turbulence is relatively high.

The mean velocity and turbulent stresses are replotted against y/y_m for the boundary-layer region in figures 18–21 and again collapse quite well onto a single curve in each case. Thus the similarity dictated by the outer flow extends well into the boundary-layer region. Moreover the shearing stress (figure 21) remains positive in this region even though $\partial u/\partial y$ becomes positive. It is interesting to note that the position of zero shear stress is at $y/y_m = 0{\cdot}3$ for $x/R = \frac{2}{3}$ and at $y/y_m = 0{\cdot}1$ for $x/R = 1$. The corresponding position for the plane case is $y/y_m = 0{\cdot}5$ and it is clear that the outer region exerts more influence on the inner layer as the curvature increases.

The longitudinal turbulence $\overline{u'^2}$ and the normal turbulence $\overline{v'^2}$ are plotted using the wall-law scaling parameters in figure 22. The results for $\overline{u'^2}/U_\tau^2$ do not collapse onto single curves and the deviation is greater for $x/R = 1$. On the other hand, the values of $\overline{v'^2}/U_\tau^2$ tend to conform to a single curve for both values of x/R. This type of behaviour is attributed by Townsend (1961) to the presence of an inactive component of turbulence which is swirling in planes parallel to the wall.

Intermittency measurements for the three cases are shown in figure 23. Results for two downstream stations are shown for the $x/R = \frac{2}{3}$ spiral, and these collapse convincingly onto a single curve. The measurement of intermittency by Giles *et al.* for an

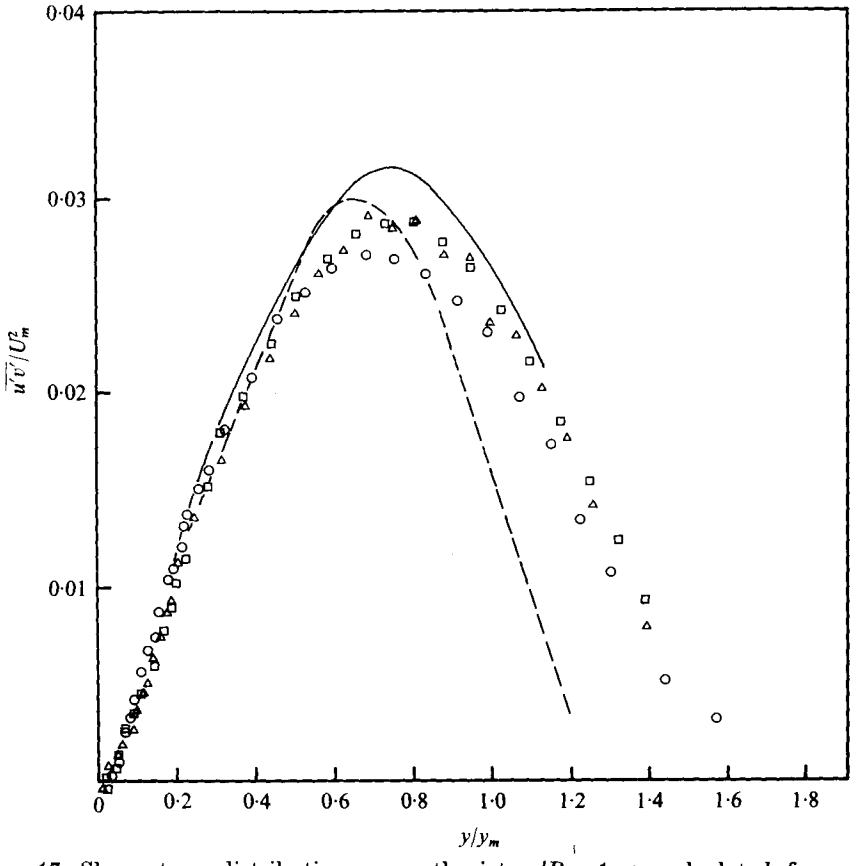

FIGURE 17. Shear-stress distribution across the jet, $x/R = 1$. *, calculated from momentum equation; ○, $x = 14{\cdot}3$ in.; □, $x = 19{\cdot}9$ in.; △, 29·8 in.; ——, mean curve through experimental points corrected for high intensity; – – –, data of Giles *et al.* (1966)

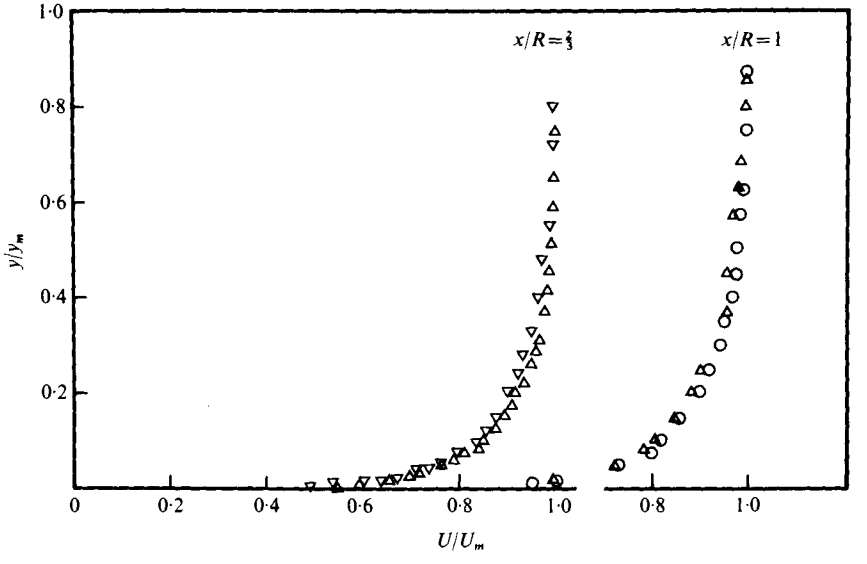

FIGURE 18. Mean velocity profile in the boundary-layer region. For $x/R = \frac{2}{3}$: ▽, $x = 13{\cdot}3$ in.; △, $x = 19{\cdot}6$ in. For $x/R = 1$: ○, $x = 14{\cdot}3$ in.; △, $x = 29{\cdot}8$ in.

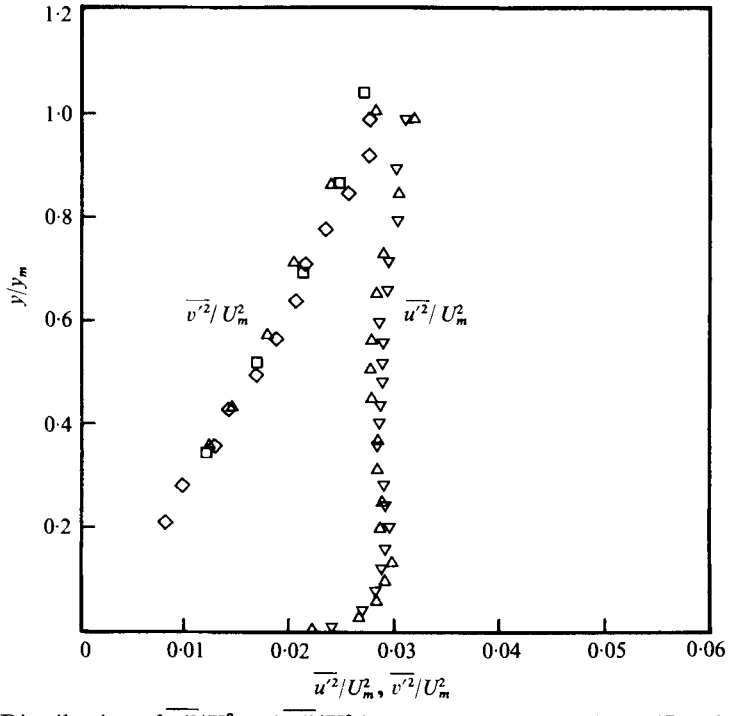

FIGURE 19. Distribution of $\overline{u'^2}/U_m^2$ and $\overline{v'^2}/U_m^2$ in boundary-layer region, $x/R = \frac{2}{3}$. △, $x = 13{\cdot}3$ in.; ▽, $x = 19{\cdot}6$ in.; □, $x = 23{\cdot}5$ in.; ◇, $x = 28{\cdot}7$ in.

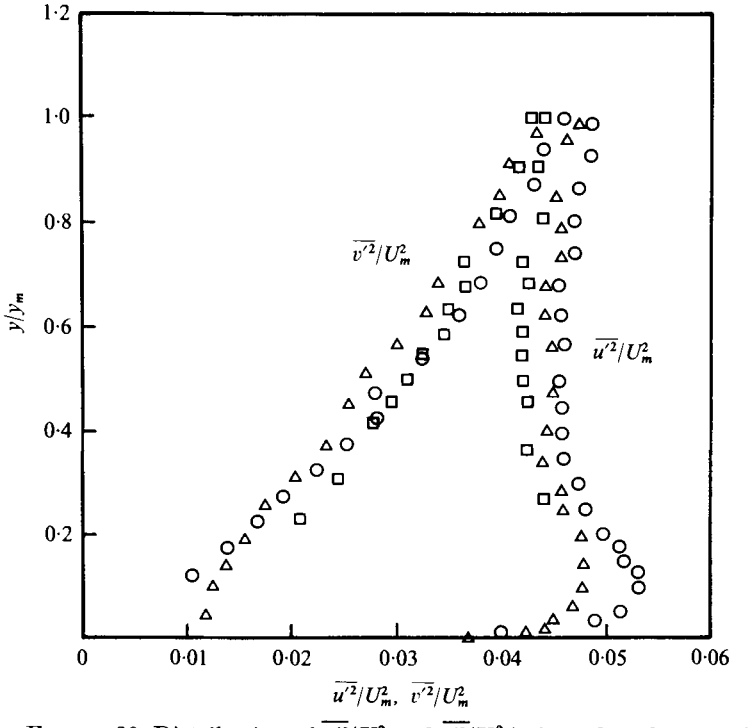

FIGURE 20. Distribution of $\overline{u'^2}/U_m^2$ and $\overline{v'^2}/U_m^2$ in boundary-layer region, $x/R = 1$. ○, $x = 14{\cdot}3$ in.; □, $x = 19{\cdot}9$ in.; △, $x = 29{\cdot}8$ in.

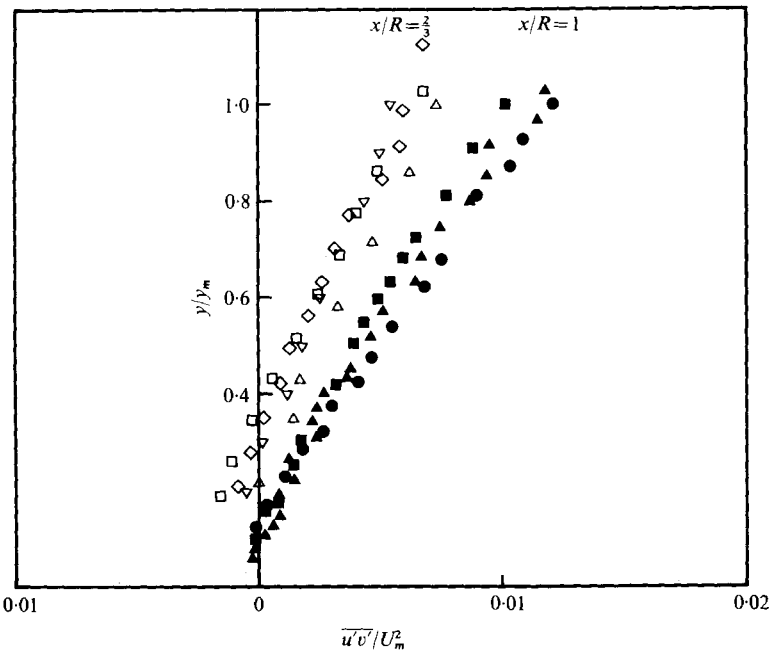

FIGURE 21. Shear-stress distribution in boundary-layer region. For $x/R = \frac{2}{3}$: △, $x = 13{\cdot}3$ in.; ▽, $x = 19{\cdot}6$ in.; □, $x = 23{\cdot}5$ in.; ◇, $x = 28{\cdot}7$ in. For $x/R = 1$: ●, $x = 14{\cdot}3$ in.; ■, $x = 19{\cdot}9$ in.: ▲, $x = 29{\cdot}8$ in.

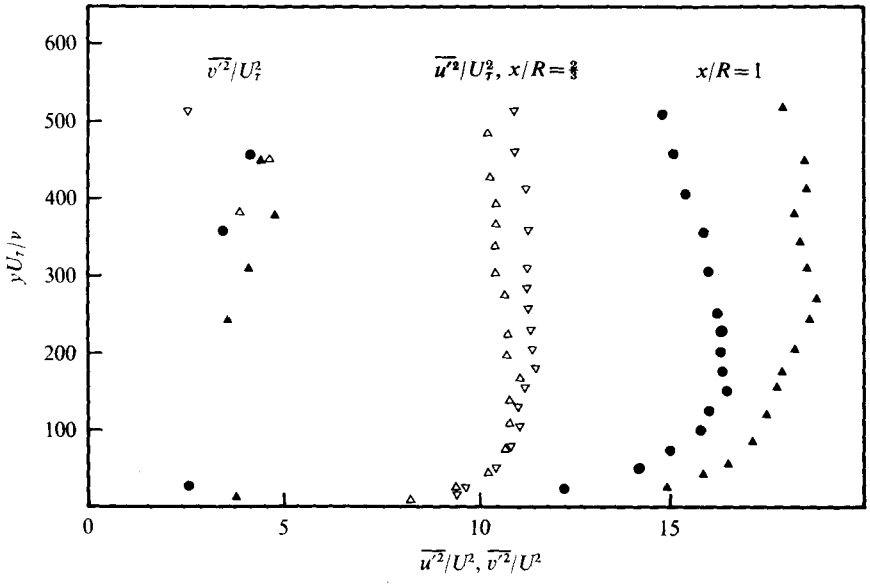

FIGURE 22. Evidence for an inactive component of turbulent motion: distribution of $\overline{u'^2}/U_\tau^2$ and $\overline{v'^2}/U_\tau^2$ in boundary-layer region. Symbols as in figure 21.

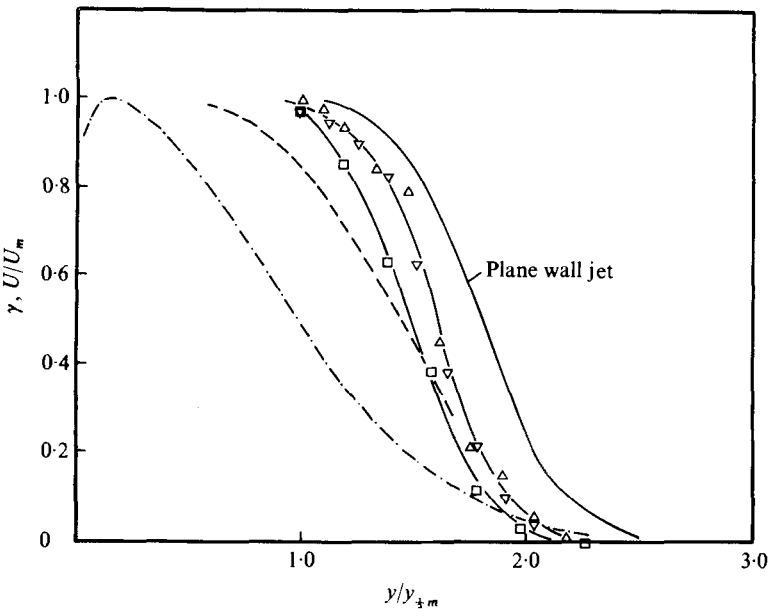

FIGURE 23. The dependence of the intermittency distribution on curvature. For $x/R = \frac{2}{3}$: △, $x = 13{\cdot}3$ in.; ▽, $x = 19{\cdot}6$ in. For $x/R = 1$: □, $x = 19{\cdot}9$ in.; – – –, data of Giles *et al.* (1966); ———, mean velocity profile.

$x/R = 1$ spiral is also shown. Disagreement with the present measurements may be noted. Some disagreement with the measurements of Giles *et al.* for a plane wall jet was also noted in a comparison which is not shown here. It is partly due to the somewhat subjective nature of the measurement itself. However, the present measurements appear to be consistent with one another. They indicate that the mean position $y_e/y_{\frac{1}{2}m}$ of the superlayer moves inwards as the curvature is increased while the relative width of the intermittent region, as measured by the standard deviation, $\sigma/y_{\frac{1}{2}m}$, is somewhat smaller for the curved flows (see figure 26).

In figure 24 the ratio $\overline{u'^2}/\overline{v'^2}$ for the three cases is plotted against $y/y_{\frac{1}{2}m}$ and the relatively large increase of $\overline{v'^2}$ due to curvature is apparent. In plane flow the turbulence production term is found only in the equation for $\overline{u'^2}$. In curved flow, however, the equation for $\overline{v'^2}$ also contains such a term. The ratio of the production term for $\overline{v'^2}$ to the production term for $\overline{u'^2}$ in curved flow (which is shown by Bradshaw (1969) to be analogous to the flux Richardson number for buoyant flow) is

$$R_f = -\left(2\overline{u'v'}\frac{u}{R+y} - \overline{v'^2}\frac{\partial v}{\partial y}\right) \Big/ \frac{\overline{u'v'}}{(R+y)}\frac{\partial}{\partial y}[u(R+y)],$$

which to $O(y_{\frac{1}{2}m}/R)$ for a self-preserving flow at $y = y_{\frac{1}{2}m}$ gives values of 0, 0·3 and 0·7 for $x/R = 0$, $\frac{2}{3}$ and 1 respectively and provides an explanation of the trends shown in figure 24.

The structure parameter $\overline{u'v'}/\overline{q'^2}$ is shown in figure 25 and appears to be insensitive to curvature within the accuracy of the present measurements. This is consistent with the assumption made by Townsend (1970).

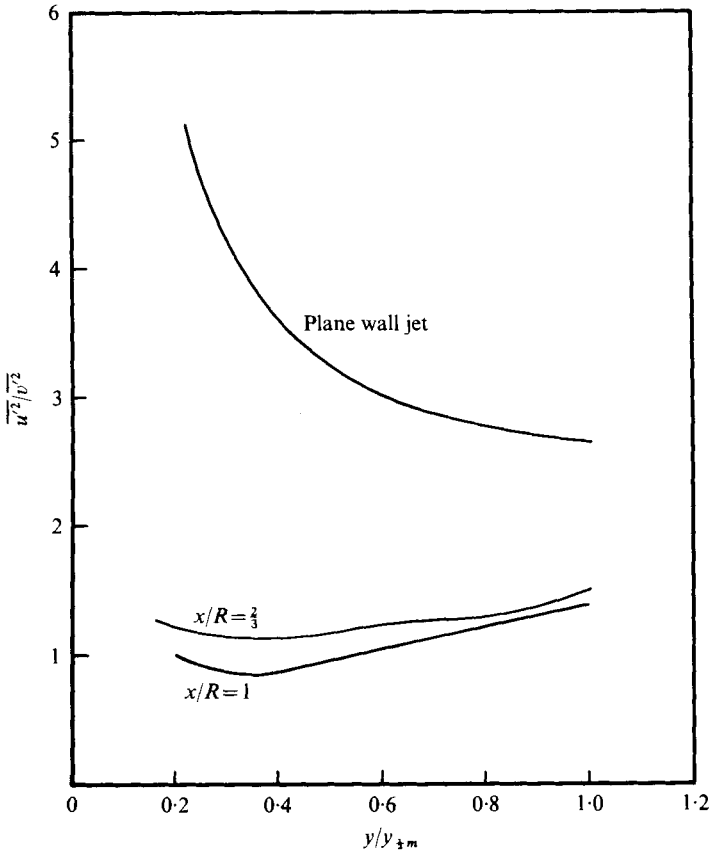

FIGURE 24. The dependence of $\overline{u'^2}/\overline{v'^2}$ on curvature.

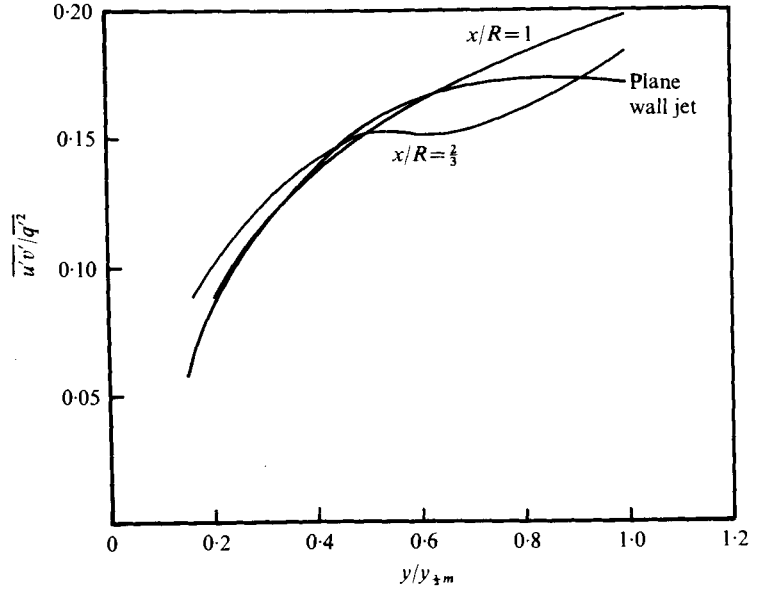

FIGURE 25. The dependence of the structure parameter $\overline{u'v'}/\overline{q'^2}$ on curvature.

$$I_{jk} = \int_0^\infty \left(\frac{y}{y_{\frac{1}{2}m}}\right)^j \left(\frac{u}{U_m}\right)^k d\left(\frac{y}{y_{\frac{1}{2}m}}\right)$$

$${}_1I_{jk} = \int_0^1 \left(\frac{y}{y_{\frac{1}{2}m}}\right)^j \left(\frac{u}{U_m}\right)^k d\left(\frac{y}{y_{\frac{1}{2}m}}\right)$$

$$I_{01} = 1{\cdot}05 \qquad {}_1I_{01} = 0{\cdot}816$$

$$I_{02} = 0{\cdot}75 \qquad {}_1I_{02} = 0{\cdot}684$$

$$I_{03} = 0{\cdot}605$$

$$I_{12} = 0{\cdot}35 \qquad {}_1I_{12} = 0{\cdot}262$$

$$I_p = \int_0^\infty \frac{u}{U_m}\left\{\int_{y/y_{\frac{1}{2}m}}^\infty \left(\frac{u}{U_m}\right)^2 d\left(\frac{y}{u_{\frac{1}{2}m}}\right)\right\} d\left(\frac{y}{y_{\frac{1}{2}m}}\right) = 0{\cdot}32$$

TABLE 2. Integrals used in the theoretical analysis and evaluated using experimentally measured velocity profiles.

Attempts have been made to predict the effect of curvature on rate of growth for these flows. Irwin & Smith (1975) have modified the model equations for the Reynolds-stress tensor developed by Launder *et al.* (1973) to account both for the presence of a wall and for small curvature. The curvature is taken to be so small that the pressure variation perpendicular to the flow is neglected in the downstream momentum equation and the predictions are in fair agreement with the measurements of Giles *et al.* for $x/R < \frac{1}{2}$. An interesting feature of Irwin & Smith's results in that the dissipation length scale is a nearly constant proportion of $y_{\frac{1}{2}m}$ and independent of the curvature. This had been previously assumed by Townsend (1970). In his theory Townsend incorporated the variation of pressure across the flow and the calculations should therefore apply for higher curvatures and be relevant to the present study.

He used the momentum equation integrated across the complete flow,

$$I_{02}\frac{dy_{\frac{1}{2}m}}{dx} + 2I_{02}\frac{y_{\frac{1}{2}m}}{U_m}\frac{dU_m}{dx} + \left(\frac{y_{\frac{1}{2}m}}{R}\right)^2 \frac{dR}{dx} I_{12} = -\frac{\tau_w}{\rho U_m^2}, \tag{12}$$

and the total energy equation, which we here also integrate across the complete flow to obtain

$$\frac{d}{dx}\left[U_m^3 y_{\frac{1}{2}m}\left(\frac{I_{03}}{2} - I_p\frac{y_{\frac{1}{2}m}}{R}\right) + U_m q_0^2 y_{\frac{1}{2}m}\frac{I_{01}}{2}\right] = -\frac{q_0^3}{L_\epsilon} y_e\left(1 + \tfrac{1}{2}\frac{y_e}{R}\right), \tag{13}$$

where the I's are integrals defined and evaluated in table 2 and the turbulent normal stresses are neglected. Also, y_e defines the half-intermittency point, q_0 is the turbulence velocity scale, defined by

$$q_0^2 = \int_0^\infty u\overline{q'^2}\,dy \Big/ \int_0^\infty u\,dy,$$

and L_ϵ is the dissipation length scale

$$q_0^3 y_e \Big/ \int_0^\infty \epsilon\,dy,$$

where ϵ is the rate of dissipation of turbulence energy per unit mass. In deriving the total energy equation, the small curvature term

$$\int_0^y \frac{y}{R}\epsilon\,dy$$

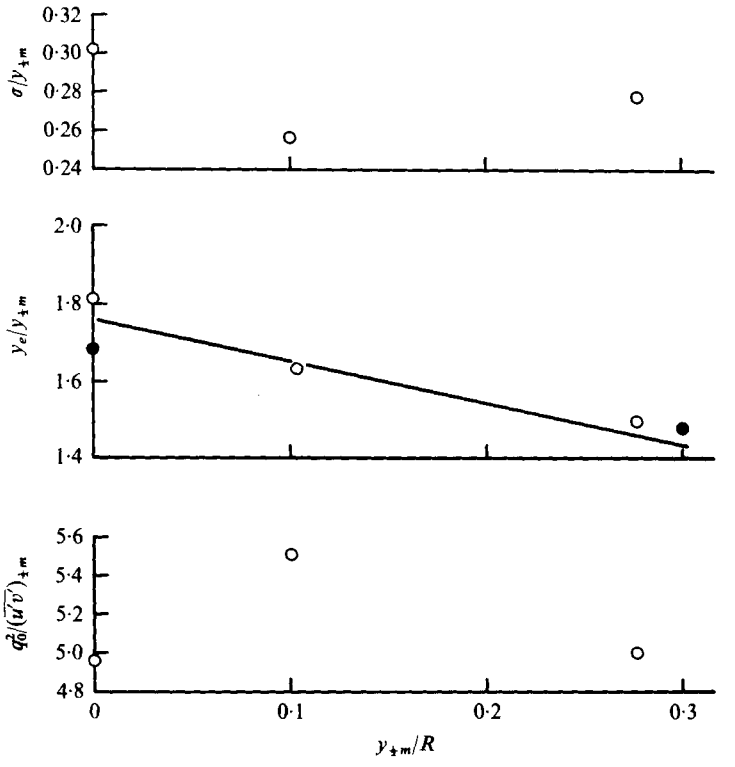

FIGURE 26. Dependence on curvature of intermittency $\sigma/y_{\frac{1}{2}m}$, edge of superlayer $y_e/y_{\frac{1}{2}m}$ and turbulence structure parameter $q_0^2/(\overline{u'v'})$.

has been derived assuming that ϵ is constant from $y = 0$ to y_e and is zero for larger values of y.

If it is assumed that $\tau_w/\rho U_m^2$, $y_e/y_{\frac{1}{2}m}$ and $L_\epsilon/y_{\frac{1}{2}m}$ are constant, and there is some support for the first two assumptions in the present measurements, then there are three unknowns: $y_{\frac{1}{2}m}$, U_m and q_0. To obtain a solution Townsend (1970) derived a third equation from the momentum equation stated at $y = y_m$. We have tried this method but it did not lead to satisfactory predictions. It has therefore been replaced by a 'half' integral momentum equation with limits $y = 0$ and $y = y_{\frac{1}{2}m}$.

Correct to order $(y_{\frac{1}{2}m}/R)^2$ this equation is

$$\frac{dy_{\frac{1}{2}m}}{dx}\left[{}_1I_{02}-\tfrac{1}{2}{}_1I_{01}+\frac{y_{\frac{1}{2}m}}{R}({}_1I_{12}-\tfrac{1}{2}{}_1I_{01})\right]+\frac{y_{\frac{1}{2}m}}{U_m}\frac{dU_m}{dx}\left[2{}_1I_{02}-\tfrac{1}{2}{}_1I_{01}+\frac{y_{\frac{1}{2}m}}{R}(2{}_1I_{02}-2I_{02}-\tfrac{1}{2}{}_1I_{01})\right]$$
$$=-\frac{(\overline{u'v'})_{\frac{1}{2}m}}{U_m^2}\left(1+\frac{y_{\frac{1}{2}m}}{R}\right)^2-\frac{\tau_w}{\rho U_m^2}. \qquad (14)$$

The full momentum equation (12) may be used to eliminate $(y_{\frac{1}{2}m}/U_m)\,dU_m/dx$ from (13) and (14) and the values of the integrals from table 2 may be inserted. Energy combined with full momentum gives

$$\left(0{\cdot}303-0{\cdot}32\frac{y_{\frac{1}{2}m}}{R}+0{\cdot}525\frac{q_0^2}{U_m^2}\right)\left(\frac{1}{2}\frac{dy_{\frac{1}{2}m}}{dx}+0{\cdot}7\left(\frac{y_{\frac{1}{2}m}}{R}\right)^2\frac{dR}{dx}+2\frac{\tau_w}{\rho U_m^2}\right) \qquad (15)$$
$$=\frac{y_{\frac{1}{2}m}}{L_\epsilon}\frac{y_e}{y_{\frac{1}{2}m}}\frac{q_0^3}{U_m^3}\left(1+\tfrac{1}{2}\frac{y_e}{y_{\frac{1}{2}m}}\frac{y_{\frac{1}{2}m}}{R}\right).$$

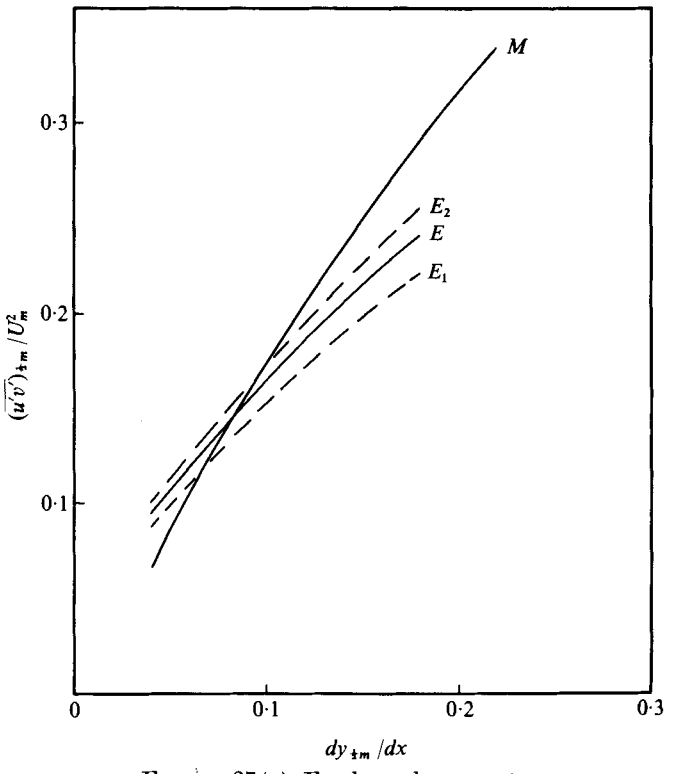

FIGURE 27 (*a*). For legend see next page.

Half-momentum combined with full momentum gives

$$\frac{dy_{\frac{1}{2}m}}{dx}\left(0{\cdot}204-0{\cdot}308\frac{y_{\frac{1}{2}m}}{R}\right)=\frac{(\overline{u'v'})_{\frac{1}{2}m}}{U_m^2}+0{\cdot}36\frac{\tau_w}{\rho U_m^2}. \tag{16}$$

Both these equations relate the rate of growth $dy_{\frac{1}{2}m}/dx$ to the shearing stress $(\overline{u'v'})_{\frac{1}{2}m}/U_m^2$ if values of $\tau_w/\rho U_m^2$, $y_{\frac{1}{2}m}/L_\epsilon$, $y_e/y_{\frac{1}{2}m}$ and $q_0^2/(\overline{u'v'})_{\frac{1}{2}m}$ may be assigned.

From figure 8, $\tau_w/\rho U_m^2$ does not vary greatly with curvature and an appropriate average value is 0·0025. Following Townsend it is assumed that $y_{\frac{1}{2}m}/L_\epsilon$ is independent of curvature (Irwin & Smith 1975). From the present measurements (figure 26) $q_0^2/(\overline{u'v'})_{\frac{1}{2}m}$ is also nearly constant. Some variation of $y_e/y_{\frac{1}{2}m}$ is observed in the present measurements (figure 26) but it is not large. Accordingly, the following values are assumed:

$$q_0^2/(\overline{u'v'})_{\frac{1}{2}m}=5{\cdot}15,\quad y_e/y_{\frac{1}{2}m}=1{\cdot}8,$$

where $y_{\frac{1}{2}m}/L_\epsilon$ is obtained from the measured rate of growth of a *plane* wall jet using (15) and (16) with $R\to\infty$. Kohan (1968) quotes values ranging from 0·06 to 0·08. The present measurements give 0·071 and this is considered to be the most plausible value. It gives $y_{\frac{1}{2}m}/L_\epsilon=0{\cdot}42$.

The solution of (15) and (16) could have been obtained by iteration. However, it is more revealing to display each equation graphically. In figure 27 the energy equation E [equation (15)] and the momentum equation M [equation (16)] are plotted for the two spirals. Three energy curves E_1, E and E_2 are shown, corresponding respectively to the

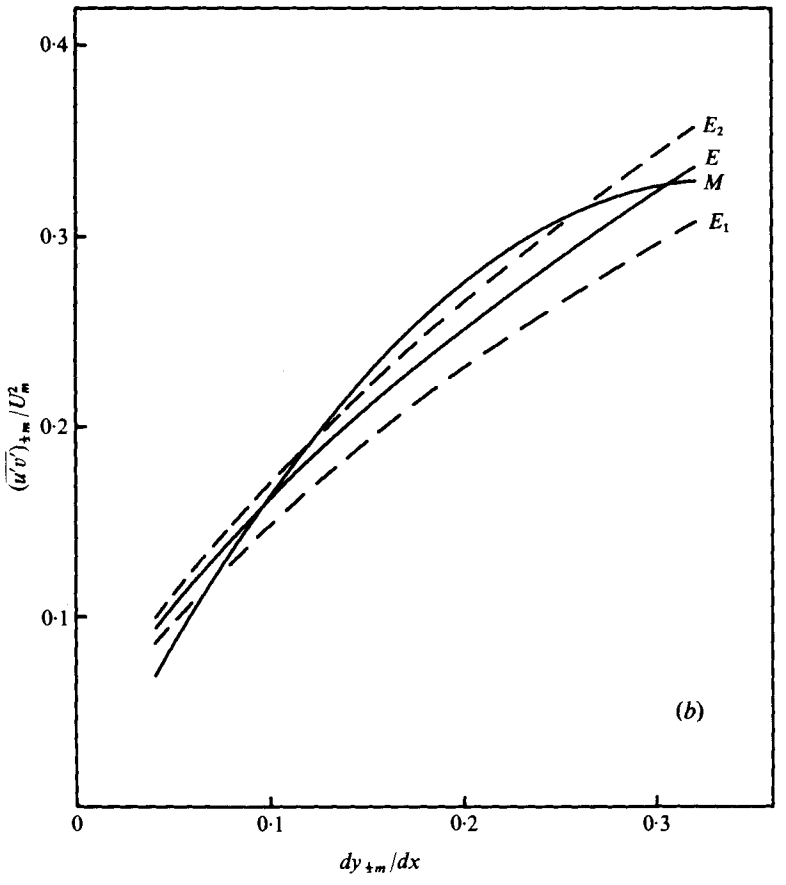

FIGURE 27. Dependence of calculated $(\overline{u'v'})_{\frac{1}{2}m}/U_m^2$ on $dy_{\frac{1}{2}m}/dx$ for (a) $x/R = \frac{2}{3}$ and (b) $x/R = 1$ spiral. Curve M is calculated using the momentum (16). Curves E_1, E and E_2 are calculated using the equation for total energy (15) and the plane wall jet growths $dy_{\frac{1}{2}m}/dx = 0{\cdot}06$, 0·071 and 0·08 respectively.

three values $dy_{\frac{1}{2}m}/dx = 0{\cdot}06$, 0·071 and 0·08 for a plane wall jet. Thus E is the most plausible curve and its intersection with M gives the predictions on the left of table 3.

The predictions are seen to be in poor agreement with the measured values. It might be mentioned that the second intersection in figure 28, although giving a larger value of $dy_{\frac{1}{2}m}/dx$, is invalid and is probably due to inaccuracy in the simplified momentum equation when the curvature is large.

To find out which of the equations is in error the *measured* values of $dy_{\frac{1}{2}m}/dx$ are used to predict the shearing stress $(\overline{u'v'})_{\frac{1}{2}m}/U_m^2$. The results are shown on the right-hand side of table 3. It is seen that much better predictions are obtained using the energy equation E, or better still E_1. The predictions from the combined momentum equations M are significantly poorer (see also figures 16 and 17). This has been convincingly attributed to a slight divergence of the flow. Thus the failure of the prediction method is mainly due to the effects of three-dimensionality, which apparently affect the half-momentum equation much more than the total energy equation, despite the simplications which have been applied to the latter.

$\frac{x}{R}$	Measured $\frac{dy_{\frac{1}{2}m}}{dx}$	Predicted $\frac{dy_{\frac{1}{2}m}}{dx}$	Measured $\frac{\overline{(u'v')}_{\frac{1}{2}m}}{U_m^2}$	Predicted $\frac{\overline{(u'v')}_{\frac{1}{2}m}}{U_m^2}$ from measured $\frac{dy_{\frac{1}{2}m}}{dx}$		
				From curve M	From curve E	From curve E_1
0	0·071	—	0·011	0·014	0·014	0·014
$\frac{2}{3}$	0·155	0·082	0·020	0·026	0·022	0·020
1	0·277	0·098	0·027	0·032	0·030	0·028

TABLE 3

5. Conclusions

(i) It has been established experimentally that wall jet flows over logarithmic spirals, with local radius proportional to surface distance, can be sensibly self-preserving. The growth rate is constant and increases significantly with the curvature of the flow. The measurements give

$$dy_{\frac{1}{2}m}/dx = 0{\cdot}071 + 0{\cdot}8\, y_{\frac{1}{2}m}/R.$$

The present curved flows have growths that are about 10 % lower than those given by previous experimenters. The maximum velocity decays according to the relation

$$U_m \propto x^a,$$

where a is slightly less than $-\frac{1}{2}$ and is a function of skin friction and curvature.

(ii) It is extremely difficult to set up a quasi-two-dimensional wall jet in which the measured shear stress agrees with that calculated from the rate of growth and the two-dimensional momentum equation. The present flows are certainly more accurate than those measured previously, nevertheless the measured and calculated shear stresses differ by 15–25 %.

(iii) The most obvious effect of curvature on the turbulence is a dramatic increase in $\overline{v'^2}$ compared with $\overline{u'^2}$. The turbulence structure parameter $\overline{u'v'}/\overline{q'^2}$ is invariant with curvature but the large eddy scale, as indicated by the mean position y_e and the standard deviation of the outer intermittency, appears to decrease slightly with increasing curvature.

(iv) Calculations using the integral equation for total energy assuming that $\overline{(u'v')}_{\frac{1}{2}m}/q_0^2$, $y_e/y_{\frac{1}{2}m}$ and $y_{\frac{1}{2}m}/L_e$ are constant indicate that the *measured* shear stress is close to what it would be in a self-preserving wall jet which was perfectly two-dimensional in the mean.

(v) The turbulence intensity is very high and linearized measurements of the turbulence stress tensor require corrections involving high-order correlations. These corrections have been applied.

(vi) The shear stress at the maximum velocity is large and of the same sign as the shear stress in the outer, jet-like, part of the flow. The turbulence in the outer flow encroaches strongly upon that in the inner boundary layer.

(vii) The conventional logarithmic law of the wall applies out to $yU_\tau/\nu = 150$ for $x/R = \frac{2}{3}$. It does not apply for $x/R = 1$. The relation between C_f and $y_m U_m/\nu$ depends slightly on curvature.

This work was supported by D.R.B. Canada under Grant number 9551–12. We are indebted to Mr P. E. Colin of the Von Kármán Institute for Fluid Dynamics for giving us some of the original apparatus which was fabricated in Brussels.

REFERENCES

ALCARAZ, E., GUILLERMET, G. & MATHIEU, J. 1968 Mésures de frottement à la paroi à l'aide de tubes de Preston et d'une balance. *C.R. Acad. Sci. Paris* A **266**, 432.

BELLHOUSE, B. J. & SCHULTZ, O. L. 1966 Determination of mean and dynamic skin friction, separation and transition in low-speed flow with a thin-film heated element. *J. Fluid Mech.* **24**, 379.

BRADSHAW, P. 1969 The analogy between streamline curvature and buoyancy in turbulent shear flow. *J. Fluid Mech.* **36**, 177.

BRADSHAW, P. 1973 Effects of streamline curvature on turbulent flow. *AGARDograph* no. 169.

BROWN, G. L. 1967 Theory and application of heated films for skin friction measurements. *Proc. Heat Trans. Fluid Mech. Inst.* (ed. D. R. Olfe & W. Van Atta), p. 361. Stanford University Press.

CLAUSER, F. H. 1954 Turbulent boundary layers in adverse pressure gradients. *J. Aero. Sci.* **21**, 91.

ESCUDIER, M. P., NICOLL, W. B. & SPALDING, D. B. 1966 An explicit drag law for uniform density turbulent boundary layers on smooth impermeable walls. *Imperial College Rep.* TWF/TN/12.

FEKETE, G. I. 1963 Coanda flow of a two-dimensional wall jet on the outside of a circular cylinder. *McGill Univ., Mech. Engng Dept. Rep.* no. 63–11.

FÖRTHMANN, E. 1934 Über turbulente Strahlausbreitung. *Ing. Arch.* **5**, 42. (Trans. *N.A.C.A. Tech. Memo.* no. 789.)

GARTSHORE, I. S. & HAWALESHKA, O. 1964 The design of a two-dimensional blowing slot and its application to a turbulent wall jet in still air. *McGill Univ., Dept. Mech. Engng Tech. Note* no. 64–5.

GIBSON, M. M. 1963 Spectra of turbulence in a round jet. *J. Fluid Mech.* **15**, 161.

GILES, J. A., HAYS, A. P. & SAWYER, R. A. 1966 Turbulent wall jets on logarithmic spiral surfaces. *Aero. Quart.* **17**, 201.

GLAUERT, M. B. 1956 The wall jet. *J. Fluid Mech.* **1**, 625.

GOLDSTEIN, S. 1938 *Modern Developments in Fluid Dynamics*, vol. 1. Oxford University Press.

GUITTON, D. 1964 Two-dimensional turbulent wall jet over curved surfaces. *McGill Univ., Dept. Mech. Engng Rep.* no. 64–7.

GUITTON, D. 1970 Some contributions to the study of equilibrium and non-equilibrium turbulent wall jets over curved surfaces. Ph.D. thesis, McGill University.

GUITTON, D. 1974 The effect of high intensity turbulence on the response of a hot wire. *C.A.S.I. Trans.* **7**, 69.

HEAD, M. R. & RECHENBERG, I. 1962 The Preston tube as a means of measuring skin friction. *J. Fluid Mech.* **14**, 1.

IRWIN, H. P. A. H. & SMITH, P. A. 1975 Prediction of the effect of streamline curvature on turbulence. *Phys. Fluids* **18**, 624.

JEROME, F. E., GUITTON, D. & PATEL, R. P. 1971 Experimental study of the thermal wake interference between closely spaced wires of a X-type hot wire probe. *Aero. Quart.* **22**, 119.

KOHAN, S. 1968 Studies of the intermittent region and the wall region of a two-dimensional plane wall jet. Ph.D. thesis, Dept. of Chemical Engineering, Stanford University.

LAUNDER, B. E., REECE, G. & RODI, W. 1973 Development and application of a Reynolds stress turbulence closure. *Imperial College, Mech. Engng Dept. Rep.* HTS/73/31. (See also *J. Fluid Mech.* **68**, 1975, 537.)

MYERS, G. E., SCHAUER, J. J. & EUSTIS, R. H. 1961 The plane turbulent wall jet. Part 1. Jet development and friction factor. *Dept. Mech. Engng, Stanford Univ. Tech. Rep.* no. 1.

NAKAGUCHI, H. 1961 Jet along a curved wall. *Dept. Aeronautics, Univ. Tokyo Res. Memo.* no. 4.

NEWMAN, B. G. 1961 The deflection of plane jets by adjacent boundaries – Coanda effect. *Boundary Layer and Flow Control.* Pergamon.

PARTHASARATHY, S. P. 1964 Two-dimensional, turbulent wall jets with and without a constant outside stream. M.Sc. thesis, Dept. of Aeronautics, Indian Institute of Science, Bangalore.

PATEL, V. C. 1965 Calibration of the Preston tube and limitations on its use in pressure gradients. *J. Fluid Mech.* **23**, 185.

SAWYER, R. A. 1962 Two-dimensional turbulent jets with adjacent boundaries. Ph.D. thesis, University of Cambridge.

SCHWARZ, W. H. & COSART, W. P. 1961 The two-dimensional turbulent wall jet. *J. Fluid Mech.* **10**, 481.

SHRIDHAR, K. & TU, P. K. C. 1969 Experimental investigation of curvature effects on turbulent wall jets. *Aero. J.* **73**, 977.

SIGALLA, A. 1958 Measurements of skin friction in a plane turbulent wall jet. *J. Roy. Aero. Soc.* **62**, 873.

SMITH, P. A. 1973 A two-dimensional jet with small curvature. Ph.D. thesis, McGill University.

SPETEL, F., MATHIEU, J. & BRISON, J. F. 1972 Tensions de Reynolds et production d'energie cinétique turbulente dans les jets pariétaux sur parois planes et concaves. *J. Méc.* **11**, 403.

TAILLAND, A. & MATHIEU, J. 1967 Jet pariétal. *J. Méc.* **6**, 103.

TOWNSEND, A. A. 1961 Equilibrium layers and wall turbulence. *J. Fluid Mech.* **11**, 97.

TOWNSEND, A. A. 1970 Entrainment and the structure of turbulent flow. Boeing Sci. Res. Lab., Symp. on Turbulence, 1969. *J. Fluid Mech.* **41**, 13,